Structure–function relationships of peptides forming the calcin family of ryanodine receptor ligands

Liang Xiao,[1,3]* Georgina B. Gurrola,[2,3]* Jing Zhang,[3] Carmen R. Valdivia,[3] Mario SanMartin,[3] Fernando Z. Zamudio,[2,3] Liming Zhang,[1] Lourival D. Possani,[2] and Héctor H. Valdivia[3]

[1]Department of Marine Biotechnology, Faculty of Naval Medicine, Second Military Medical University, Shanghai 200433, China
[2]Departamento de Medicina Molecular y Bioprocesos, Instituto de Biotecnología, Universidad Nacional Autónoma de México, Cuernavaca, Morelos 62271, México
[3]Center for Arrhythmia Research, Cardiovascular Division, Department of Internal Medicine, University of Michigan, Ann Arbor, MI 48109

Calcins are a novel family of scorpion peptides that bind with high affinity to ryanodine receptors (RyRs) and increase their activity by inducing subconductance states. Here, we provide a comprehensive analysis of the structure–function relationships of the eight calcins known to date, based on their primary sequence, three-dimensional modeling, and functional effects on skeletal RyRs (RyR1). Primary sequence alignment and evolutionary analysis show high similarity among all calcins (≥78.8% identity). Other common characteristics include an inhibitor cysteine knot (ICK) motif stabilized by three pairs of disulfide bridges and a dipole moment (DM) formed by positively charged residues clustering on one side of the molecule and neutral and negatively charged residues segregating on the opposite side. [^{3}H]Ryanodine binding assays, used as an index of the open probability of RyRs, reveal that all eight calcins activate RyR1 dose-dependently with K_d values spanning approximately three orders of magnitude and in the following rank order: opicalcin$_1$ > opicalcin$_2$ > vejocalcin > hemicalcin > imperacalcin > hadrucalcin > maurocalcin >> urocalcin. All calcins significantly augment the bell-shaped [Ca^{2+}]-[^{3}H]ryanodine binding curve with variable effects on the affinity constants for Ca^{2+} activation and inactivation. In single channel recordings, calcins induce the appearance of a subconductance state in RyR1 that has a unique fractional value (~20% to ~60% of the full conductance state) but bears no relationship to binding affinity, DM, or capacity to stimulate Ca^{2+} release. Except for urocalcin, all calcins at 100 nM concentration stimulate Ca^{2+} release and deplete Ca^{2+} load from skeletal sarcoplasmic reticulum. The natural variation within the calcin family of peptides offers a diversified set of high-affinity ligands with the capacity to modulate RyRs with high dynamic range and potency.

INTRODUCTION

Excitation–contraction coupling is the process that facilitates Ca^{2+} release from the SR of cardiac or skeletal muscle fibers after electrical excitation of the surface/transverse (t-) tubule membrane (Tanabe et al., 1988; Bers, 2002). During this process, the release of Ca^{2+} from the SR is caused by the activation of the Ca^{2+} release channel/ryanodine receptors (RyRs), which form homotetrameric assemblies and constitute the largest ion channels known to date, with molecular masses of ~2.2 MD and each monomer consisting of ~5,000 amino acid residues (Lai et al., 1988; Yuchi et al., 2012). In mammals, RyRs are expressed in three different forms, which help them gain the functional flexibility to respond to different triggering signals: RyR1 (Takeshima et al., 1989) is predominantly expressed in fast- and slow-twitch skeletal muscle and in cerebellar Purkinje cells; RyR2 (Nakai et al., 1990) is found in cardiac muscle but is also robustly expressed in brain and in visceral and arterial smooth muscle; RyR3 (Hakamata et al., 1992) is the least understood of the RyR isoforms and appears to play its most important role during development, although in mature cells is found in diaphragm, epithelial cells, brain, and smooth muscle (Fill and Copello, 2002). Structurally, the RyR channel is the center of a massive macromolecular complex whose function is modulated by secondary messengers (Ca^{2+}, Mg^{2+}, ATP) and accessory proteins (e.g., calmodulin, FK506-binding protein, sorcin, triadin, junctin, calsequestrin; Bers, 2004; Ather et al., 2013).

Exogenous chemicals and peptides binding to RyRs and modulating their activities have become invaluable tools for the structural and functional profiling of RyRs as well as the development of new drugs for RyR-associated diseases. The plant alkaloid ryanodine, for which this receptor was named, binds RyRs preferentially in the open state (Sutko et al., 1997), which allows experimenters to use [^{3}H]ryanodine as a high-affinity (nanomolar) probe of the functional state of

*L. Xiao and G.B. Gurrola contributed equally to this paper.
Correspondence to Héctor H. Valdivia: hvaldiv@umich.edu
Abbreviations used in this paper: DM, dipole moment; ED, evolutionary distance; ICK, inhibitor cysteine knot; PSA, polar surface area; RyR, ryanodine receptor; TFA, trifluoroacetic acid.

© 2016 Xiao et al. This article is distributed under the terms of an Attribution–Noncommercial–Share Alike–No Mirror Sites license for the first six months after the publication date (see http://www.rupress.org/terms). After six months it is available under a Creative Commons License (Attribution–Noncommercial–Share Alike 3.0 Unported license, as described at http://creativecommons.org/licenses/by-nc-sa/3.0/).

The Rockefeller University Press $30.00
J. Gen. Physiol. 2016 Vol. 147 No. 5 375–394
www.jgp.org/cgi/doi/10.1085/jgp.201511499

The Journal of General Physiology

Downloaded from http://rupress.org/jgp/article-pdf/147/5/375/1795506/jgp_201511499.pdf by guest on 07 February 2026

the channel. Ryanodine was instrumental in the isolation of the RyR1 and RyR2 channels and continues to aid in the characterization of key pharmacologic properties of RyRs, although some undesirable features like concentration-dependent biphasic effects, slow association and dissociation rate (which make its effect practically irreversible), loss of affinity upon derivatization, etc. hamper its use in cellular and biochemical settings. Caffeine is another classical ligand of RyRs with low affinity (K_d ~300 µM) that is widely used to assess the presence and size of RyR-gated Ca^{2+} stores by increasing the sensitivity of RyR channels to both cytosolic and luminal Ca^{2+} (Rousseau and Meissner, 1989; Kong et al., 2008) and eliciting Ca^{2+} release. Other ligands like doxorubicin (Abramson et al., 1988), tetracaine (Curran et al., 2007), ruthenium red (Lukyanenko et al., 2000), K201 (Wehrens et al., 2004), and carvedilol (Zhou et al., 2011) bind to and modulate the activity of RyRs, helping to "tame" their activity in pathological settings (Valdivia, 2014).

Except for ryanodine at low concentrations, all of the aforementioned ligands of RyRs exhibit off-target effects. In search of novel ligands of RyRs with high affinity and specificity, we found in the venom of selected scorpions peptides that selectively mobilize Ca^{2+} from RyR-gated stores. Imperatoxin A (from the scorpion *Pandinus imperator*) is a small (3.7-kD), highly basic (pI 8.9), globular, and thermostable peptide that activates RyRs with high affinity ($K_d \approx 5$–10 nM) and specificity (no other target proteins known to date; Valdivia et al., 1992; El-Hayek et al., 1995; Zamudio et al., 1997; Nabhani et al., 2002). Imperatoxin A spawned the discovery of calcins, a small but growing group of scorpion peptide agonists of RyRs, and to conform to its structural and functional characteristics, we hereby rename it imperacalcin, which also avoids confusion with other scorpion toxin blockers of ion channels. The defining functional feature of calcins is their capacity to stabilize RyR openings in a long-lasting, subconductance state (Tripathy et al., 1998). This effect is nearly analogous to that of ryanodine, but unlike ryanodine, calcins bind rapidly to RyRs (fast association rate), freely dissociate from their binding site (reversible effect), display a dose- and sequence-variable effect, and are amenable for derivatization without undergoing major loss in receptor affinity (El-Hayek et al., 1995; Samsó et al., 1999; Shtifman et al., 2000; Dulhunty et al., 2004; Gurrola et al., 2010). As a native family of intracellular RyR ligands, calcins are also appealing by their capacity to penetrate cell membranes with high efficiency, resulting in extremely rapid effects (lag time 2–3 s) on intracellular Ca^{2+} signaling, as indicated by an acute increase in the amplitude of the $[Ca^{2+}]_i$ transient, indicative of enhanced Ca^{2+} release from the SR (Schwartz et al., 2009; Gurrola et al., 2010). Moreover, calcins are capable of carrying large, membrane-impermeable cargo across the plasma membrane, a finding with exciting implications for intracellular drug delivery (Altafaj et al., 2005; Boisseau et al., 2006), particularly in the treatment of RyR channelopathies (Benkusky et al., 2004).

Despite the importance of calcins as selective, high-affinity membrane-permeable ligands of RyRs, key structural features of this family of scorpion peptides remain unclear, and there are no studies to date that have systematically investigated the role of their structural domains in relation to RyR affinity and single RyR channel effects. Here we present all native calcins known to date, including four previously reported (imperacalcin, maurocalcin, hemicalcin, and hadrucalcin), three previously uncharacterized (opicalcin$_1$, opicalcin$_2$, and urocalcin), and one novel (vejocalcin) peptides, and provide a comprehensive analysis of their structure–function relationship based on primary sequence examination, physicochemical characterization, three-dimensional structure modeling, and their functional effects on RyR1 channels using [^{3}H]ryanodine binding, single channel recordings, and Ca^{2+} release from SR vesicles. Natural variations in the calcin family of peptides offer a diversified set of RyR ligands with the capacity to modulate RyR channels with variable potency and high dynamic range.

MATERIALS AND METHODS

Animals

Animal care and handling conformed to the Guide for Care and Use of Laboratory Animals published by the US National Institutes of Health (NIH publication no. 85-23, revised 1996), and experimental protocols were approved by the local institutional ethical committee. The New Zealand White rabbits used in this study were maintained in environmentally controlled rooms with 12-h light/dark cycles and adequate food and water, where they was assessed daily for wellbeing by trained veterinary personnel. Back and leg skeletal muscle was obtained after intraperitoneal injection of 100 mg/kg pentobarbital. Adequacy of anesthesia was assessed by pedal reflex and evaluation of jaw and muscle tone before proceeding with surgery (Schwartz et al., 2009).

Venom source and purification procedures for vejocalcin

Venom from *Vaejovis mexicanus* (Scorpiones: Vaejovidae) for vejocalcin was obtained in the laboratory by electrical stimulation (15–25 V, 3 ms) in the articulation of the telson (last post-abdominal segment). Scorpions were milked using a Grass stimulator. The venom was collected in Eppendorf LoBind tubes and, when needed, dissolved in double-distilled water and then centrifuged at 14,000 *g* for 15 min at 4°C. The soluble supernatant was either lyophilized or stored at −20°C and later separated by HPLC essentially as described

Downloaded from http://rupress.org/jgp/article-pdf/147/5/375/1795506/jgp_201511499.pdf by guest on 07 February 2026

previously (Schwartz et al., 2006). In brief, whole venom was injected into a C18 reverse-phase semi-preparative column (Vydac) and separated by using a linear gradient from solvent A (0.12% trifluoroacetic acid [TFA] in water) to 60% solvent B (0.10% TFA in acetonitrile) run for 60 min at a flow rate of 1 ml·min^{-1}. The fractions of interest from several independent runs were pooled and further purified on a C18 reverse-phase analytic column (Vydac) to obtain vejocalcin in homogeneous form, as shown by mass spectrometry analysis and amino acid sequencing.

Amino acid sequence determination and mass spectrometry analysis

The amino acid sequence of vejocalcin was obtained by automatic Edman degradation in an LF 3000 Protein Sequencer (Beckman Coulter) using the chemicals and procedures previously described for other peptides of scorpion venom (Schwartz et al., 2006). The molecular mass of vejocalcin was obtained by mass spectrometer analysis, using an LCQ Duo (Finnigan), also as described previously (Schwartz et al., 2006).

Chemical synthesis, folding, and purification of calcins

Calcins were synthesized by an automated peptide synthesizer (Applied Biosystems model 432A) as described previously (Zamudio et al., 1997; Seo et al., 2011). In brief, a linear analogue of calcin (imperacalcin, for example) was synthesized by the solid-phase methodology with Fmoc–amino acids. After cleavage with 90% TFA for 4 h at room temperature, the crude linear peptide was extracted with 5% acetic acid and dried by vacuum centrifugation. The cyclization reaction to form disulfide bonds in the molecule was performed in the folding buffer (20 mM Na_2HPO_4 + 0.1 M NaCl + 5 mM GSH + 0.5 mM GSSG). After pH adjustment to 7.9 with 1 M NaOH, the reaction mixture was allowed to oxidize at room temperature for 4 h. After oxidation of the disulfide bonds, the peptide solution was acidified with formic acid to pH 3.0 and pumped onto a C18 column. The sample was eluted with a linear gradient from 0 to 60% B in 60 min (buffer A = H_2O containing 0.12% TFA, and buffer B = acetonitrile containing 0.1% TFA). Finally, the resulting peptide was analyzed by mass spectrometry and amino acid sequence. Peptide purity was >98% for all calcins.

Rabbit skeletal heavy SR preparation

Heavy SR vesicles were purified from rabbit white back and leg skeletal muscle, as described previously (Meissner, 1984; Dyck et al., 1987). Protein concentration was measured by the Bradford method.

[^{3}H]Ryanodine binding assay

[^{3}H]Ryanodine binding to rabbit skeletal SR was performed as described previously (El-Hayek et al., 1995; Gurrola et al., 1999; Schwartz et al., 2009). In brief, calcins were diluted directly into the incubation medium (0.2 M KCl, 10 µM $CaCl_2$, and 10 mM Na-HEPES, pH 7.2) to achieve a final concentration of 1 pM to 20 µM, as indicated in graphs. To determine the effect of calcins on Ca^{2+} sensitivity of [^{3}H]ryanodine binding activity, each calcin was added at fixed concentration (100 nM) to the standard incubation medium, which contained 0.2 M KCl, 1 mM Na_2EGTA, 10 mM Na-PIPES, pH 7.2, and $CaCl_2$ to set free [Ca^{2+}] in the range of 10 nM to 10 mM. The Ca^{2+}/EGTA ratio was calculated with the computer program MAXCHELATOR. [^{3}H]Ryanodine (95 Ci·mmol^{-1}; PerkinElmer) was diluted directly in the incubation medium to a final concentration of 5 nM. Protein concentration of heavy SR was 0.3 mg·ml^{-1} and was determined by the Bradford method. Incubation lasted 120 min at 36°C. 100-µl samples were always run in duplicate, filtered on GF/C glass filters (Whatman) and washed twice with 5 ml of distilled water using an M24-R cell harvester (Brandel). Nonspecific binding was determined in the presence of 20 µM unlabeled ryanodine, reached no more than 5–10% of the total binding, and was subtracted from each sample.

Single channel recordings

Single channel recordings of rabbit skeletal RyR1 incorporated into planar lipid bilayers were performed as described previously (Schwartz et al., 2009). Planar lipid bilayers, composed of phosphatidylethanolamine (Avanti Polar Lipids, Inc.) and phosphatidylserine (Avanti Polar Lipids, Inc.; 1:1), were painted with a glass rod across an aperture of 150-µm diameter in a Delrin cup. The cis chamber represented the cytosolic side, which was held at virtual ground and contained the reference electrode. The trans chamber corresponded to the luminal side and contained the voltage command electrode. Electrodes were connected to the head stage of a 200A Axopatch amplifier. Both the cis (0.7 ml) and trans (0.7 ml) chambers were filled with 300 mM caesium methanesulphonate and 20 mM MOPS, pH 7.2. Cs^+ was selected as the charge carrier to increase the channel conductance and to avoid any contribution from potassium channels present in the SR membrane. Chloride channels were inhibited by using the impermeant anion methanesulfonate. Contaminant Ca^{2+}, determined by a Ca^{2+} electrode, was ≈5 µM and served to activate RyR1 channels. Heavy SR vesicles (20–50 µg) were added to the cis chamber. Channel recordings were collected at different holding potentials (40 mV) before and after the addition of calcins. Single channel recordings were filtered with an 8-pole low-pass Bessel filter set at 2 kHz and digitized at a rate of 4 kHz by using a Digidata 1440A AD/DA interface. Data acquisition and analysis were performed with Axon Instruments hardware and software (pCLAMP 10) and graphed by using Microcal Inc. Origin 9.0.

Downloaded from http://rupress.org/jgp/article-pdf/147/5/375/1795506/jgp_201511499.pdf by guest on 07 February 2026

SR Ca^{2+} release measurements

Ca^{2+} release from heavy SR was measured using the Ca^{2+}-sensitive dye Arsenazo III (Sigma-Aldrich), modified as previously described (Gurrola et al., 1999; Chen et al., 2003). In brief, the absorbance was monitored at 650 nm by a compact UV-visible spectrophotometer (BioPhotometer Plus; Eppendorf). Heavy SR vesicles (20 µg) were actively loaded with Ca^{2+} at room temperature in a 1-ml basal buffer containing 100 mM KCl, 7.5 mM sodium pyrophosphate, and 20 mM MOPS, pH 7.0, supplemented with 25 µM Arsenazo III, 1 mM ATP/$MgCl_2$ (Sigma-Aldrich), 5 mM creatine phosphate disodium salt tetrahydrate (ICN Biomedicals Inc.), and 12 µg/ml creatine phosphokinase (porcine heart; EMD Millipore). Ca^{2+} loading was started by consecutive additions of 50 nmol twice and 20 nmol thrice of $CaCl_2$ before the addition of calcins. The total [Ca^{2+}] loaded into the SR was quantified by the addition of the Ca^{2+} ionophore A23187 (5 µM), and the absorbance was converted to nmol [Ca^{2+}] by a standard curve generated by sequential additions of $CaCl_2$ (10–20 µM).

Bioinformatics

Five calcin sequences (mature peptide and/or precursors), namely opicalcin$_1$ (P60252; Zhu et al., 2003), opicalcin$_2$ (P60253; Zhu et al., 2003), maurocalcin (P60254; Fajloun et al., 2000), hadrucalcin (B8QG00; Schwartz et al., 2009), and urocalcin (AGA82762; Luna-Ramírez et al., 2013), were obtained by similarity with imperacalcin (formerly imperatoxin A; P59868; Zamudio et al., 1997) with BLAST search. The exact mature sequences were further confirmed from their original papers. The sequence of hemicalcin was obtained from the corresponding paper (Shahbazzadeh et al., 2007). Vejocalcin was purified and sequenced from its natural venom in the current study. Multiple sequence alignment tool Clustal Omega was used to align the calcin sequences and analyze their identity. Evolutionary history, using the "minimum evolution" method (Kumar, 1996), was conducted in MEGA 5.2 (Tamura et al., 2011). The evolutionary distance (ED) was computed using the Poisson correction method starting from the assumption that the rate of amino acid substitution at each site follows the Poisson distribution. Physical and chemical characterization, net charge versus pH plots, and hydrophobicity plots were analyzed by ProtParam, WebLab, ViewerPro, and the online peptide calculator (http://www.chinapeptides.com/tool.php?isCalu=1) in their corresponding functions. The secondary structures were analyzed by Ramachandran plots according to the structure of imperacalcin (MMDB ID: 23273), which was first resolved by NMR (Lee et al., 2004). Similarly, using imperacalcin as template, three-dimensional simulation was performed by Swiss-PdbViewer 4.1.0 with the mutagenesis function following the minimum energy principle. Discovery Studio 3.5 was used to display the modeling molecules. Solvent-accessible polar surface area (PSA) for each calcin was calculated by using the molecular visualization program PyMOL (DeLano Scientific), and the dipole moment (DM) was analyzed by the online Protein Dipole Moments Server.

Statistics

Statistical analyses were performed by using either the computer software program Origin (version 9.0) or SigmaStat computer software (version 5.0; Rockware Inc.). Data are presented as the mean ± SEM. Data were compared using a one-way ANOVA. Differences of $P < 0.05$ between sample means were considered significant.

Online supplemental material

Fig. S1 shows the backbone structure of the eight calcins. Fig. S2 shows the dose–response effect of imperacalcin on single RyR channel kinetics. Table S1 lists the amino acid composition of all eight known calcins. Online supplemental material is available at http://www.jgp.org/cgi/content/full/jgp.201511499/DC1.

RESULTS

Isolation and primary structure determination of vejocalcin

Initial fractionation of soluble venom from *V. mexicanus* by HPLC separated >60 different components (Fig. 1 A). The fraction eluting at 20.96 min (vejocalcin) was further purified in an analytical C18 reverse-phase column, yielding the component of interest (Fig. 1 B, peak labeled with asterisk). Mass spectrometry analysis of this peak revealed a single peptide with 3,774.92 atomic mass units (a.m.u.). Amino acid sequence of the reduced and alkylated peptides yielded a single sequence up to residue 25. The digestion of reduced vejocalcin with AspN-endopeptidase permitted separation by HPLC of several subpeptides that under sequence analysis by Edman degradation and mass spectrometry fragmentation allowed the elucidation of a unique primary structure. An AspN-endopeptidase peptide yielded the overlapping sequence from position D^{15} to R^{33}. The theoretical mean mass of the amino acid sequence shown in Fig. 1 C is 3,774.5 $(M+H)^+$, which corresponds well with the experimental value of the native peptide. We have termed this peptide according to the genus of the scorpion and their great similarity to other peptide members of the calcin family (see Fig. 2).

Amino acid sequence alignment and evolutionary analysis of the calcin family

Fig. 2 A shows the amino acid sequence of all peptide members of the calcin family known to date. All calcins are made up of 33 amino acids, except hadrucalcin, which prolongs its N terminus by adding Ser and Glu for

Downloaded from http://rupress.org/jgp/article-pdf/147/5/375/1795506/jgp_201511499.pdf by guest on 07 February 2026

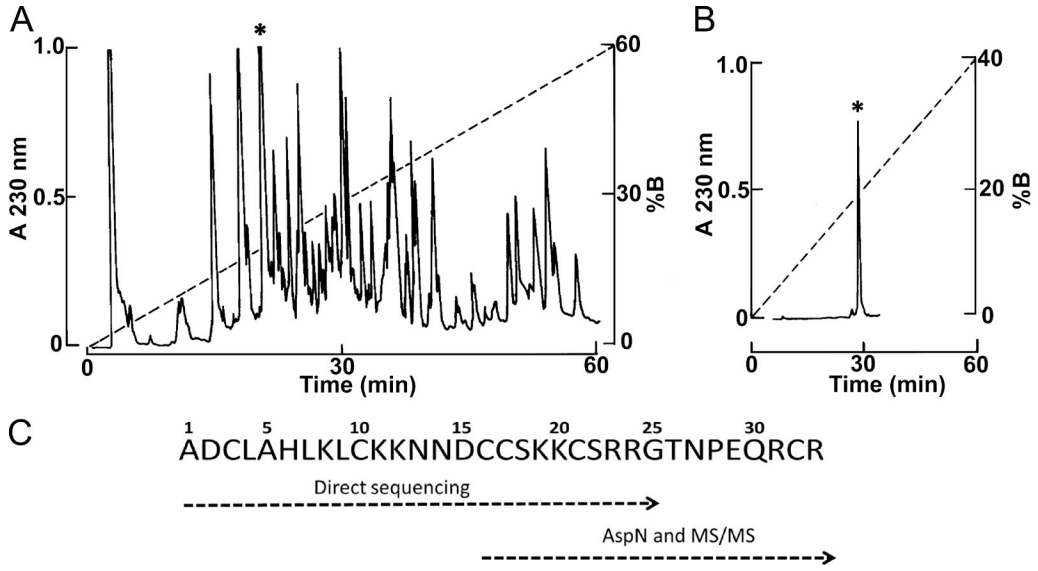

Figure 1. **Purification and characterization of vejocalcin.** (A) 1.5 mg of soluble venom from *V. mexicanus* was separated by HPLC using a semi-preparative C18 reverse-phase column, eluted with a linear gradient from solution A to 60% solution B, run for 60 min. The fraction labeled with the asterisk was rechromatographed in an analytical C18 reverse-phase column and run from solution A to 40% solution B in 60 min. (B) The component with retention time of 28.09 min (marked with an asterisk) is vejocalcin. (C) The complete amino acid sequence of vejocalcin was obtained by a combination of direct Edman degradation and mass spectrometry, as described in Materials and methods.

a total of 35 residues. Six cysteines are highly conserved and may be used for precise alignment of these peptides; i.e., the number of residues interspaced between cysteines is identical for all calcins. Determination of disulfide bonds in maurocalcin (Mosbah et al., 2000) and imperacalcin (Lee et al., 2004) indicates that the pairings Cys^{3}-Cys^{17}, Cys^{10}-Cys^{21}, and Cys^{16}-Cys^{32} (Fig. 2 B) contribute significantly to the inhibitor cysteine knot (ICK) motif (see Fig. S1) that characterizes this family of peptides. In terms of homology, calcins may be grossly split into halves for a distinctive pattern of variation: the N-terminal segment ^{1}G-N^{14} contains only four residues that are identical in all calcins (two of them are cysteines), whereas the C-terminal segment ^{15}D-R^{33}, comprising the highly positively charged motifs ^{19}KKCKRR^{24} and ^{30}KRCR^{33}, is relatively conserved among calcins (there are only nine variations in a total of 152 amino acids; 13 columns of amino acids are identical). Thus, by primary sequence analysis only, one might be tempted to estimate the hierarchical role of calcins domains, with the C-terminal half playing a prominent role based on high similarity. However, this hierarchy may turn equivocal because the overall variation of calcins is relatively minor, with identity descending only to 78.8% in the case of hadrucalcin. Also, as will be shown in three-dimensional representations of calcins, variable segments may intertwine with highly conserved segments, breaking up what may be considered "canonical" domains.

Fig. 2 C shows the evolutionary relationship of the calcin family obtained with the minimum evolution method. The evolutionary value was determined with the Poisson correction method, where 0 and 1 represent identity and divergence, respectively, between two molecules. Opicalcin$_2$ is naturally the closest to opicalcin$_1$ (only one residue different) with ED value = 0.015. In the middle, imperacalcin, hemicalcin, and maurocalcin display a similar ED to opicalcin$_1$ (0.065), followed by vejocalcin with ED = 0.123. Urocalcin and hadrucalcin are the farthest and hence the most divergent among calcins; yet the ED is still small, with maximal ED = 0.142, indicating that the ancestor of this family of peptides is relatively close to these eight known calcins.

Physicochemical features of calcins

The molecular mass of calcins ranges from 3,758.5 D (imperacalcin) to 4,190.8 D (hadrucalcin), whereas the molecular volume falls between 2,692.7 Å^3 (vejocalcin) and 3,001.9 Å^3 (hadrucalcin; Table 1). As for the composition of amino acids (Fig. 2 and Table S1), positively charged residues Lys and Arg are abundant and range from 9 (27%) for vejocalcin to 13 (39%) for urocalcin. Conversely, negatively charged residues Asp and Glu are sparse, ranging from three (9%) for vejocalcin to five (14%) for hadrucalcin. This high positive/negative amino acid ratio gives calcins high isoelectric point (pI = 9.3–10.1) and net positive charge at pH 7.0 that ranges from 5.8 (vejocalcin) to 8.7 (urocalcin). By the same token, the richness of charged residues determines the excellent solubility in water of calcins (hydrophilicity = 0.7–1.2) despite the fact that they are membrane permeable and should intuitively be hydrophobic in nature. However, as is the case for most membrane-permeable

Downloaded from http://rupress.org/jgp/article-pdf/147/5/375/1795506/jgp_201511499.pdf by guest on 07 February 2026

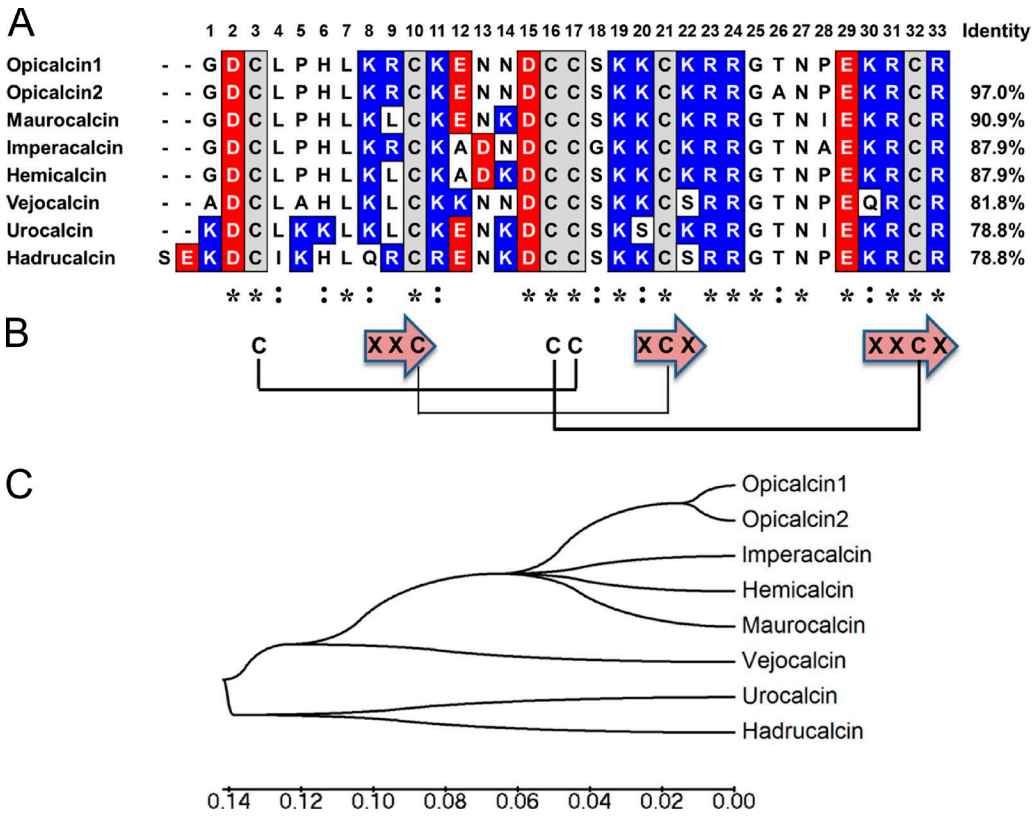

Figure 2. **Calcin sequence alignment and evolutionary analysis.** (A) The eight calcins known to date are aligned with opicalcin$_1$ as reference by Clustal Omega. The identity values to opicalcin$_1$ are shown on the right side. Positively charged residues lysine (K) and arginine (R), negatively charged residues aspartic acid (D) and glutamic acid (E), and the disulfide bond-forming cysteine (C) are highlighted by the colors blue, red, and gray, respectively. Columns with identical residue are marked by asterisks, whereas columns with only one difference are marked by colons on the bottom. (B) Three pairs of highly conserved disulfide bonds (Cys^3-Cys^{17}, Cys^{10}-Cys^{21}, and Cys^{16}-Cys^{32}) and the residues forming part of β strands appear connected to form an ICK motif. (C) The evolutionary tree is built with the principle minimum evolution by MEGA 5.2. The genetic distance is measured by Poisson correction method with the formula $d_{AB} = -\ln(1 - f_{AB})$, where f_{AB} is the fraction of different amino acids after the Poisson distribution between two sequences (dissimilarity).

peptides, hydrophilicity and membrane permeability may be oddly compatible. The most notable deviation from the group is vejocalcin, which holds the lowest pI (9.3), poorest hydrophilicity (0.7), and least positive charges at pH 7.0 (5.8). On the other extreme, urocalcin has the highest number of positively charged residues (13) and the highest pI (10.1), is the most hydrophilic (1.2), and holds the most charges at pH 7.0 (8.7; Table 1 and Fig. 3, A and B). As we will discuss, both extremes turn out to be detrimental for receptor affinity.

Secondary and spatial structures of the calcin family of peptides

The three-dimensional structures of maurocalcin (Mosbah et al., 2000) and imperacalcin (Lee et al., 2004) have been determined by ^{1}H-NMR. We used their structural templates and modeled the six remainder calcins as described in Materials and methods (only imperacalcin-modeled structures are presented; similar results were obtained using maurocalcin as a template). All calcins are predicted to fold into an ICK motif, whose defining features include the presence of three disulfide bridges along with sections of polypeptide between them forming β strands. In the case of calcins, the first (Cys^3-Cys^{17}) and the second (Cys^{10}-Cys^{21}) disulfide bonds form a loop, through which the third (Cys^{16}-Cys^{32}) disulfide bond passes across, forming a knot (hence the term cysteine knot; Fig. 4 and Fig. S1). Accordingly, calcins contain three β strands and one α helix interspaced between β strands 1 and 2 (βαββ). β strands 2 and 3 form an antiparallel sheet (Table 2 shows that that ^{20}KCK^{22}, the second β strand, is ^{20}KCS^{22} in vejocalcin, thus reducing its propensity to form β strand 2). The ICK motif confers to these peptides a globular, highly stable structure that is likely responsible for their resistance to heat denaturation and proteolysis. Despite their coiled, compact globular structure, the solvent-accessible PSA of calcins is relatively high, owing to their abundance of negatively and positively charged residues, ranging from 2,721 Å^2 (imperacalcin) to 2,965 Å^2 (urocalcin). Hadrucalcin breaks into the PSA >3,000 Å^2 because of its additional N-terminal

Downloaded from http://rupress.org/jgp/article-pdf/147/5/375/1795506/jgp_201511499.pdf by guest on 07 February 2026

Table 1. **Physical and chemical characteristics of calcins**

Calcins	Formula	Amino acids	Molecular mass	Molecular volume	Negatively charged residues	Positively charged residues	Theoretical isoelectric point	Hydrophilicity	Ratio of hydrophilic residues	Net charge at pH 7.0	PSA
			D	*Å*^{3}							*Å*^{2}
OpCa1	$C_{153}H_{261}N_{59}O_{47}S_6$	33	3,871.5	2,762.6	4 (12%)	11 (33%)	9.7	1.1	58%	6.8	2,761
OpCa2	$C_{152}H_{259}N_{59}O_{46}S_6$	33	3,841.5	2,742.0	4 (12%)	11 (33%)	9.7	1.1	58%	6.8	2,733
IpCa	$C_{148}H_{254}N_{58}O_{45}S_6$	33	3,758.4	2,783.7	4 (12%)	11 (33%)	9.7	1.0	52%	6.8	2,721
MCa	$C_{156}H_{270}N_{56}O_{46}S_6$	33	3,858.6	2,781.9	4 (12%)	11 (33%)	9.6	1.0	55%	6.8	2,821
HmCa	$C_{153}H_{263}N_{55}O_{45}S_6$	33	3,785.5	2,721.9	4 (12%)	11 (33%)	9.6	1.0	52%	6.8	2,765
VjCa	$C_{149}H_{254}N_{56}O_{47}S_6$	33	3,774.4	2,692.7	3 (9%)	9 (27%)	9.3	0.7	55%	5.8	2,790
UrCa	$C_{158}H_{282}N_{56}O_{47}S_6$	33	3,910.7	2,840.9	4 (12%)	13 (39%)	10.1	1.2	64%	8.7	2,965
HdCa	$C_{164}H_{282}N_{64}O_{53}S_6$	35	4,190.8	3,001.9	5 (14%)	12 (34%)	9.7	1.2	66%	6.8	3,227

Summary of the physical and chemical characteristics of all eight known calcins, including formula, quantity of amino acids, molecular mass, molecular volume, negatively and positively charged amino acids, theoretical isoelectric point, hydrophilicity, ratio of hydrophilic residues, and net charge at pH 7.0. HdCa, hadrucalcin; HmCa, hemicalcin; IpCa, imperacalcin; MCa, maurocalcin; OpCa1, opicalcin$_1$; OpCa2, opicalcin$_2$; UrCa, urocalcin; VjCa, vejocalcin.

Downloaded from http://rupress.org/jgp/article-pdf/147/5/375/1795506/jgp_201511499.pdf by guest on 07 February 2026

polar amino acids Ser and Glu, which stick out prominently from the main protein core (Fig. 4 H).

Another distinguishing feature of calcins is their segregated arrangement of charged residues, where most of the positively charged amino acids are clustered in one side of the molecule, whereas neutral and negatively charged residues crowd the opposite side (Fig. 4), generating a discrete DM. The best examples of this segregated electrostatic distribution are imperacalcin (Fig. 4 A), opicalcin$_1$ (Fig. 4 B), and opicalcin$_2$ (Fig. 4 C), with DM (in Debye lengths [D]) = 152, 173, and 175 D, respectively. As observed, the "frontal" side of these calcins presents the majority (but not all) of the basic residues that form part of clusters ^{8}KRCK^{11}, ^{19}KKCKRR^{24}, and ^{30}KRCR^{33}, whereas the "dorsal" side presents only neutral and acidic residues, creating a largely negative sector that is electrically countered only in the flanks by basic residues. On the other extreme, vejocalcin (Fig. 4 F) and hadrucalcin (Fig. 4 H) exhibit the smallest charge segregation, with DM = 40 and 65 D, respectively. In these calcins, disruption of basic clusters by neutral and acidic residues in the frontal side of the molecules and, conversely, encroachment of basic residues in the negative sector of the dorsal side contribute substantially to equalize the spatial distribution of electrical charges. Interestingly, imperacalcin and hadrucalcin both penetrate isolated ventricular myocytes and induce intracellular Ca^{2+} release with comparable kinetics (Schwartz et al., 2009; Gurrola et al., 2010), indicating that a large DM is not required for calcins to enter cells and exert their pharmacological effect. We tested direct interaction of calcins with RyR1 using [^{3}H]ryanodine binding assays to determine whether DM is instead related to calcin affinity for RyRs (see next section).

Calcins stimulate [^{3}H]ryanodine binding in a dose-dependent manner and at all Ca^{2+} levels

We compared side by side the property of all eight calcins to stimulate [^{3}H]ryanodine binding to RyR1, the skeletal isoform of RyRs (Fig. 5) and contrasted their effect with that of caffeine. Imperacalcin, the founder member of the calcin family, was discovered by its capacity to activate [^{3}H]ryanodine binding to RyR1 (Valdivia et al., 1992). Three other calcins have since been characterized, namely, maurocalcin, hemicalcin, and hadrucalcin (Zamudio et al., 1997; Fajloun et al., 2000; Shahbazzadeh et al., 2007; Schwartz et al., 2009), which also stimulate [^{3}H]ryanodine binding to RyR1. Opicalcin$_1$ and opicalcin$_2$ (Zhu et al., 2003) as well as urocalcin (Luna-Ramírez et al., 2013) and vejocalcin (this study) have never been tested for biological activity. As expected from their structural homology, all calcins stimulate [^{3}H]ryanodine binding to RyR1, but also as expected from their unique amino acid sequence, they exhibit different affinity (apparent K_d; Fig. 5 A) and potency (maximal stimulation as percentage of control; Fig. 5 B). The apparent K_d surprisingly spanned ≈3 orders of magnitude, with the following ranking order (nM): opicalcin$_1$ 0.3 ± 0.04 > opicalcin$_2$ 3.2 ± 0.4 > vejocalcin 3.7 ± 0.4 > hemicalcin 6.9 ± 0.7 > imperacalcin 8.7 ± 0.9 > hadrucalcin 14.8 ± 1.9 > maurocalcin 26.4 ± 3.9 >> urocalcin 376 ± 45 (mean ± SEM; n = 3–5). Especially remarkable are opicalcin$_1$ and opicalcin$_2$, which differ by only one amino acid (the highly conserved Thr^{26} is replaced by Ala in opicalcin$_2$), yet they display an ≈10-fold difference in K_d. An identical replacement in synthetic imperacalcin also decreases its K_d by ≈10-fold (Gurrola et al., 1999), indicating that Thr^{26} forms part, or is close to, the active site of calcins. Another notable deviation is urocalcin, with the lowest K_d of all calcins but with multiple variations in apparently key domains of calcins (see Discussion).

We also tested the effect of calcins over a wide range of [Ca^{2+}] to determine how they affect the Ca^{2+}-dependent activation and inactivation of RyR1 (Fig. 5, B–E). Specific binding in the absence of calcins (Fig. 5 B, control, black squares) had a threshold for detection at 100 nM [Ca^{2+}] (pCa 7) and was maximal at 10–100 µM [Ca^{2+}] (pCa 5–4). Higher [Ca^{2+}] decreased binding. This dual effect of Ca^{2+} gave rise to a typical bell-shaped

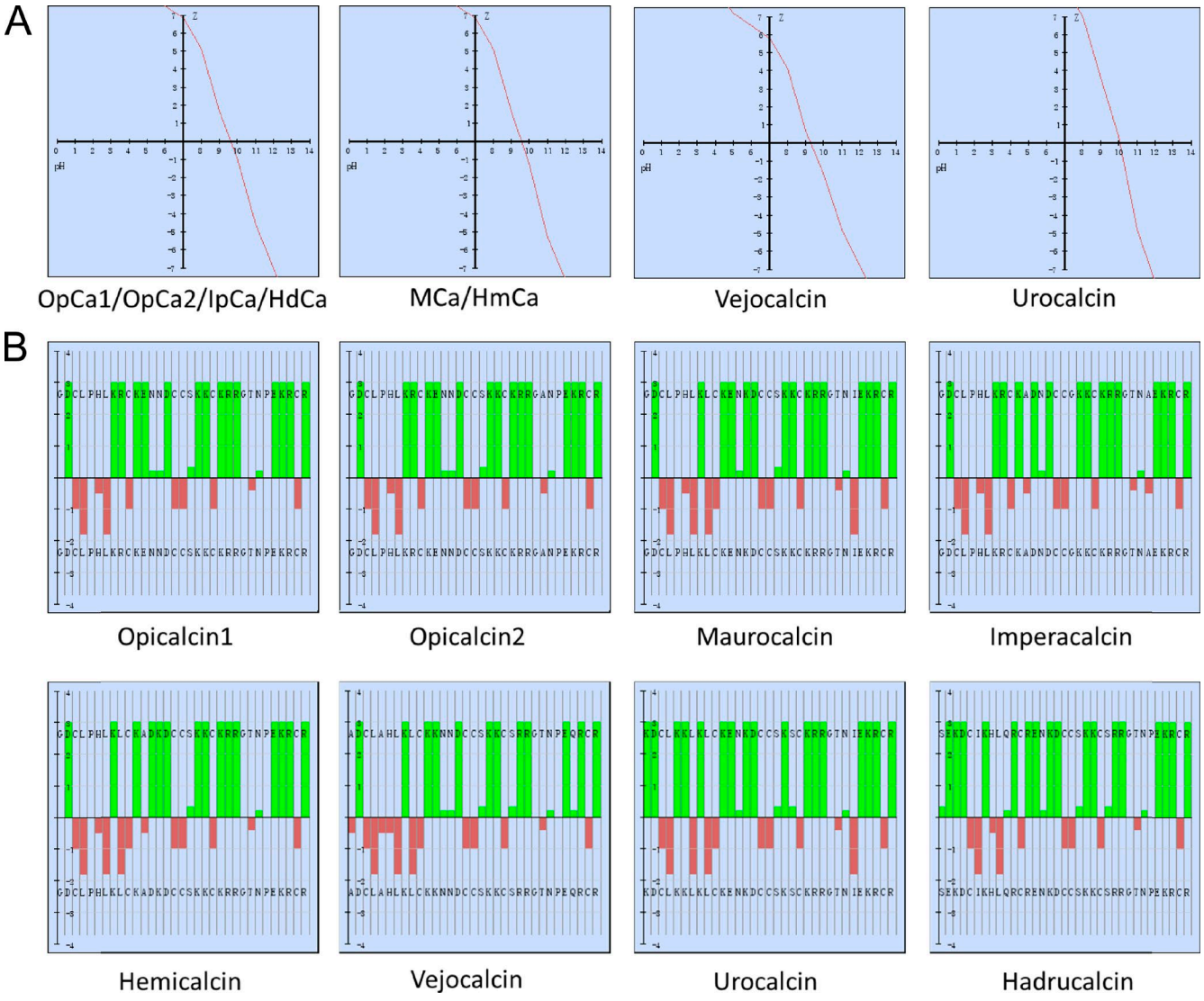

Figure 3. **Net charge versus pH plot and hydrophobicity plot of calcins.** (A) Net charge versus pH plot of calcins. The theoretical isoelectric points of calcins are highly basic with values ranging from 9.3 (vejocalcin) to 10.1 (urocalcin), whereas the net charges at pH 7.0 are positive for all calcins and vary from 5.8 (vejocalcin) to 8.7 (urocalcin). (B) Hydrophobicity plot of calcins. The ratio of hydrophilic residues (green) of calcins is between 52% (imperacalcin and hemicalcin) and 66% (hadrucalcin), indicating high solubility in water for all calcins.

curve, which could be fitted with the equation $B = ((B_{max} \cdot [Ca^{2+}])/(K_a + [Ca^{2+}]) \cdot (K_i/(K_i + [Ca^{2+}]))$, where B = specific binding, B_{max} is the maximal amount of binding (normalized to 100% in the absence of calcins), and K_a (558 ± 116 nM) and K_i (389 ± 86 µM) represent the apparent affinity of Ca^{2+} to an activation and inactivation site, respectively. In the presence of a near-saturating concentration of calcin (3 µM for urocalcin and 100 nM for the remainder calcins), the binding curve was also bell-shaped, but it was dramatically augmented in absolute values (Fig. 5 B). In general, the augmentation of [^{3}H]ryanodine binding produced by calcins increased with [Ca^{2+}], the threshold for activation decreased to ≈*p*Ca 8, and the optimal binding shifted to ~*p*Ca 5. Thus, for all calcins except vejocalcin, K_a was lower than control and ranged between ~50 and 530 nM [Ca^{2+}], indicating that calcins potentiate the activating effect of Ca^{2+} on RyR1 (Fig. 5, C–E). Conversely, more [Ca^{2+}] was required to inactivate RyR1 in the presence of calcins; thus, K_i was invariably lower than control, ranging from 0.42 ± 0.05 (vejocalcin) to 5.52 ± 0.64 (urocalcin) mM [Ca^{2+}]. In contrast, 3 mM caffeine increased almost exclusively the ascending limb of the curve, i.e., it "sensitized" RyRs to activating Ca^{2+} (Fig. 5 B); hence, K_a is exclusively affected with negligible effect on K_i (Fig. 5 C). Thus, in contrast to caffeine, calcins widen both limbs of the Ca^{2+}-dependent [^{3}H]ryanodine binding curve of RyR1, indicating that they act by different mechanisms. If [^{3}H]ryanodine binding is proportional to channel activity (Pessah et

Downloaded from http://rupress.org/jgp/article-pdf/147/5/375/1795506/jgp_201511499.pdf by guest on 07 February 2026

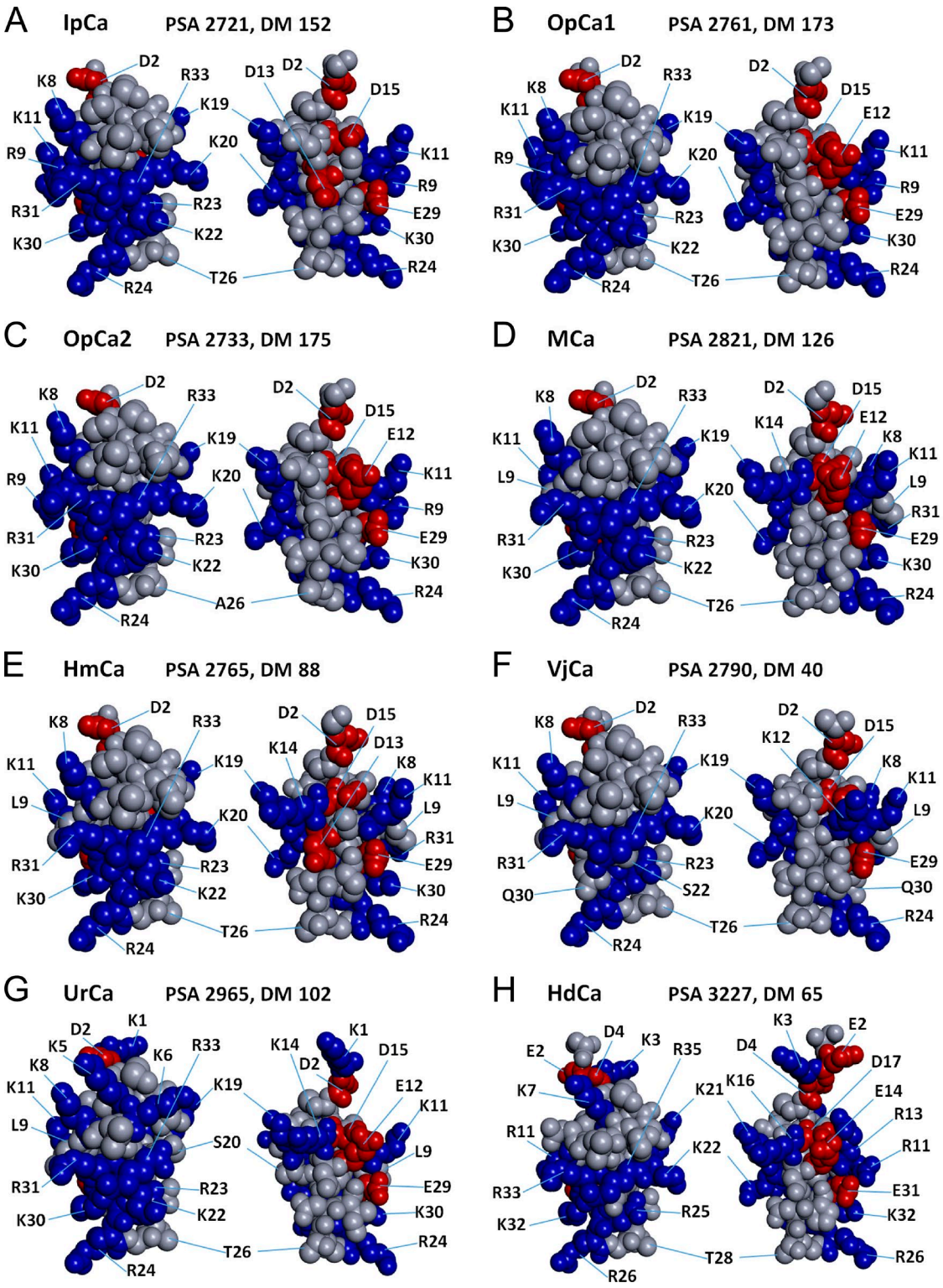

Figure 4. **Three-dimensional modeling of calcins.** (A) Imperacalcin, resolved by ^{1}H-NMR (Lee et al., 2004), was taken as the template molecule. (B–H) Other calcins, including opicalcin$_1$ (B), opicalcin$_2$ (C), maurocalcin (D), hemicalcin (E), vejocalcin (F), urocalcin (G), and hadrucalcin (H), were simulated by Swiss-PdbViewer 4.1.0 and viewed by Discovery Studio 3.5. Solvent-accessible PSAs were calculated using PyMOL, whereas DMs were analyzed by the online Protein Dipole Moments Server. For each calcin, the solid ribbon with line atom model may be found in Fig. S1, and the charged CPK model with frontal side (middle) and dorsal side (right) are displayed here. Positively charged residues (Lys and Arg), negatively charged residues (Asp and Glu), and neutral residues are colored by blue, red, and gray, respectively.

Downloaded from http://rupress.org/jgp/article-pdf/147/5/375/1795506/jgp_201511499.pdf by guest on 07 February 2026

Table 2. **Imperacalcin-based secondary structure prediction**

Calcins	Secondary structure (amino acids)			
	β sheet1 (8–10)	β sheet2 (20–22)	β sheet3 (30–33)	3/10-helix (13–15)
OpCa1	KRC	KCK	RCR	NND
OpCa2	KRC	KCK	RCR	NND
MCa	KLC	KCK	RCR	NKD
IpCa	KRC	KCK	RCR	DND
HmCa	KLC	KCK	RCR	DKD
VjCa	KLC	–	RCR	NND
UrCa	KLC	SCK	RCR	NKD
HdCa	QRC	KCS	RCR	NKD

Three β sheets (8–10, 20–22, and 30–33) and one 3/10-helix (13–15) are predicted for all calcins except vejocalcin, which lacks the β2 sheet. HdCa, hadrucalcin; HmCa, hemicalcin; IpCa, imperacalcin; MCa, maurocalcin; OpCa1, opicalcin$_1$; OpCa2, opicalcin$_2$; UrCa, urocalcin; VjCa, vejocalcin.

al., 1987), the results indicate that calcins, too, bind to a conformational-sensitive state of the channel, requiring Ca^{2+} to open the channel and expose its binding site (see Discussion).

Single channel recordings

To further investigate the functional properties of calcins, we reconstituted RyR1 channels in planar lipid bilayers and determined the effect of calcins on single channel gating. Because a full description of the imperacalcin effect on single RyR1 channel gating has already been provided (Tripathy et al., 1998), followed by isolated accounts on maurocalcin (Mosbah et al., 2000), hemicalcin (Shahbazzadeh et al., 2007), and hadrucalcin (Schwartz et al., 2009) effects also on the RyR1 channel, our main goal here was to compare the amplitude of the subconductance state induced by each calcin under identical experimental conditions and to relate this effect to their physicochemical characteristics (Fig. 6). Because the probability of calcin binding to RyR1 is P_o and voltage dependent (Tripathy et al., 1998), we conducted experiments at "P_o-clamped" conditions (by fixing $[Ca^{2+}]$ at quasi-optimal levels) and positive holding potential (40 mV), which favor the natural (lumen to cytosol) flow of ions through RyRs. Under these conditions, control (no calcin) RyR1 channel recordings showed the characteristic fast-flickering (mean open time 1–3 ms), low P_o (0.03–0.15), and high-conductance (≈600 pS) gating, with occasional sojourns to native subconducting states that were barely noticeable in the current amplitude histogram (Fig. 6 A). There were also bursts of high P_o, reflecting the characteristic intermodal gating of all RyR isoforms (Rosales et al., 2004). Calcins (100 nM each) all interacted with RyR1 and induced a "signature" event, consisting of long-lasting, reversible, transient subconductance state. However, fractional conductance of the calcin-induced event differed for each peptide. Opicalcin$_1$ (Fig. 6 B) and opicalcin$_2$ (Fig. 6 C) induced subconductance states corresponding to 0.35 and 0.40 of the full-conductance level, respectively. Imperacalcin (Fig. 6 D), maurocalcin (Fig. 6 E), and hadrucalcin (Fig. 6 F) induced substates of fractional value that are in good agreement with those previously reported, i.e., 0.30 (Tripathy et al., 1998), 0.48 (Fajloun et al., 2000), and 0.35 (Schwartz et al., 2009) of full conductance state, respectively. However, the subconducting state induced by hemicalcin (Fig. 6 G) was only 0.20 in our hands, which is lower than the 0.38 value previously reported (Shahbazzadeh et al., 2007). The subconductance position induced by vejocalcin was the highest, with a value of 0.60 (Fig. 6 H). In contrast, urocalcin induced a subconductance state = 0.55, but in line with its low affinity in [^{3}H]ryanodine binding assays (Fig. 5 A), it was difficult to detect it at concentrations similar to the other calcins (100 nM), so we increased its concentration to 1 µM (Fig. 6 I) in this assay.

To better ascertain whether calcins bind exclusively to the open state of the RyR, as postulated before (Tripathy et al., 1998; Lukács et al., 2008), we performed additional single channel experiments using increasing and nonsaturating concentrations of imperacalcin and examined (a) the probability of substate conductance, (b) the mean open and mean closed times of the channel in "bursting mode" (calcin-free), and (c) the mean duration of the subconductance state (calcin dwelling time). Fig. S2 A shows representative single RyR1 channel recordings in the presence of 5, 30, and 100 nM imperacalcin, and Fig. S2 C shows the probability of substate occurrence ($P_{substate}$) as a function of [imperacalcin]. The data can be fitted by a hyperbolic function, and a Lineweaver–Burk plot (not depicted) indicates that the data fit Michaelis–Menten-type kinetics with a maximal $P_{substate}$ close to 1.0 and a K_d = 12 nM (in very close agreement to the [^{3}H]ryanodine binding assay of Fig. 5 A). Mean open and mean closed times of the channel in bursting mode or those in the "calcin mode" (obtained by exponential fits of the bursts in the fully conducting or subconducting channel, respectively) were not significantly modified by [imperacalcin], indicating that the kinetics of gating of the calcin-free channel remain impervious to [imperacalcin] as expected and, more importantly, that the dwelling time of imperacalcin is also unaffected by [imperacalcin]. Thus, a simplified scheme emerges, in

Downloaded from http://rupress.org/jgp/article-pdf/147/5/375/1795506/jgp_201511499.pdf by guest on 07 February 2026

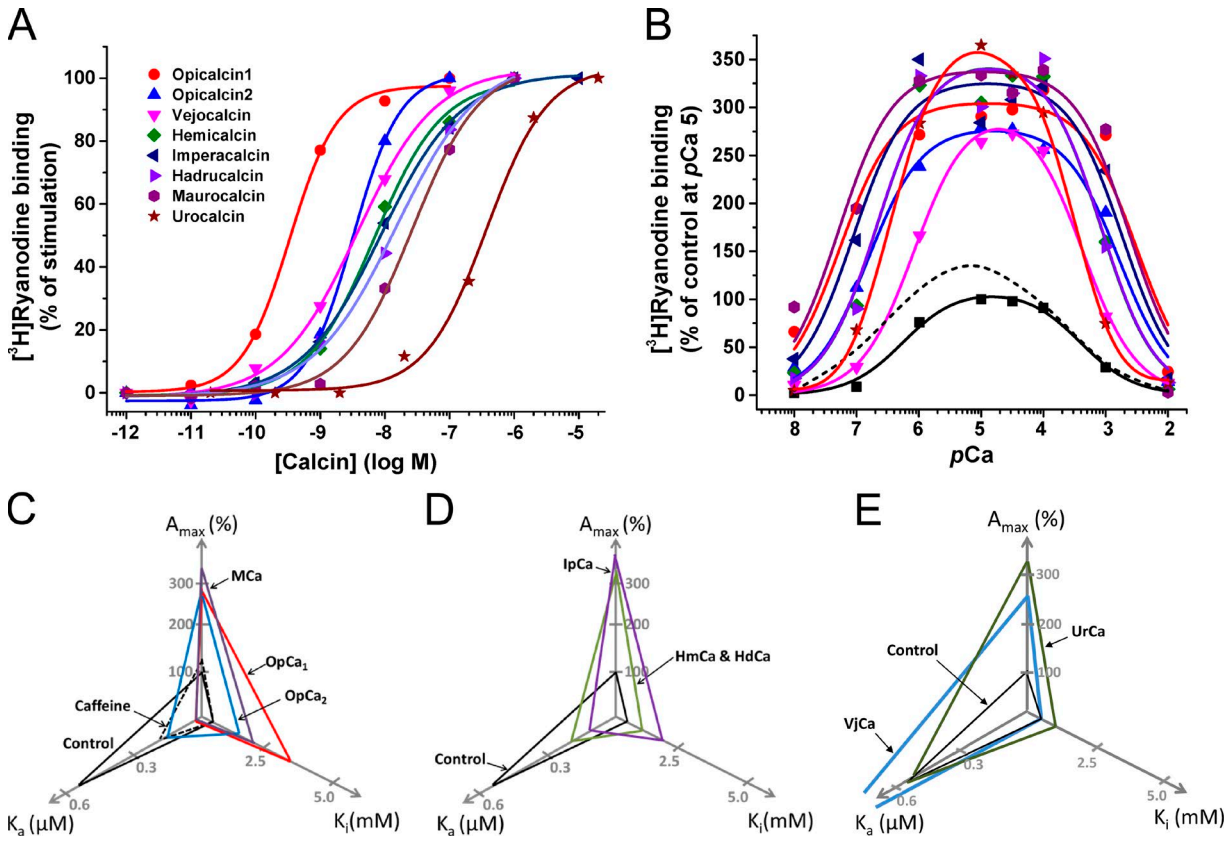

Figure 5. **[^{3}H]Ryanodine binding stimulation by calcins.** (A) Dose-dependent activation of RyR1 by calcins, with boundaries set at 1 pM to 20 μM (n = 3–5). Heavy SR from rabbit skeletal muscle was incubated with 5 nM [^{3}H]ryanodine in the absence (control) and the presence of the indicated concentrations of calcins. Binding conditions were specified in Materials and methods. The K_d was determined with the formula $B = (B_{max})/[1 + (K_d/[calcin])^{nH})$, where B is specific binding of [^{3}H]ryanodine, B_{max} is the maximum binding stimulated by calcin, and nH is the Hill coefficient. (B) Effect of calcins (100 nM each; n = 3–5) on the Ca^{2+}-dependent [^{3}H]ryanodine binding curve. Ca^{2+}-dependent activation and inactivation were fitted with the formula $B = ((B_{max}\cdot[Ca^{2+}])/(K_a + [Ca^{2+}]))\cdot(K_i/(K_i + [Ca^{2+}]))$, where B is the specific binding of [^{3}H]ryanodine, B_{max} is the maximum binding stimulated by calcin, K_a is the activation constant, and K_i is the inactivation constant. The specific [^{3}H]ryanodine binding was standardized with the value of the control at pCa5 as 100%. (C–E) Radar charts illustrating the effect of calcins on K_a, K_i, and maximal amplitude (A_{max}; percentage of stimulation with respect to control). The black line corresponds to control (no calcin) and is included in all charts for reference. Caffeine (C, dashed line) moves K_a but has little effect on A_{max} and no effect on K_i. This effect contrasts with that of calcins (C–E, color lines as indicated), which affect K_a, K_i, and A_{max}.

which the RyR transits between close (C) and open (O) states and calcins bind to the open channel to produce a calcin-modified RyR ($O_{substate}$), as follows:

$$C \leftrightarrow O \leftrightarrow O_{substrate}.$$

Because $P_{substate}$ follows Michaelis–Menten-type kinetics and is strictly dependent on [imperacalcin], the *on* reaction $O \rightarrow O_{substate}$ corresponds to k_{on}, the bimolecular process governed by open RyR · [imperacalcin]. Conversely, the *off* reaction $O \leftarrow O_{substate}$ is independent of [imperacalcin] and corresponds to a process governed exclusively by the intrinsic properties of calcin binding to the channel. Because the *off* reaction is the same at low and saturating concentration of imperacalcin, this strongly suggests that, at least within the range of [imperacalcin] tested, the process is unimolecular, that is, only one calcin dissociates from the channel after inducing the substate. Thus, we favor the notion that only one calcin molecule is required to exert the "signature effect" of these group of peptides.

We also analyzed single channel recordings and visually inspected each of 48 calcin-induced subconductance states in the channel of Fig. S2 A, at 100 nM imperacalcin. We scored 1 for each channel transition from discretely open to subconducting (open, on) and the same for a transition from subconducting to discretely open again (open, off; examples marked by asterisks in Fig. S2 B) and 0 for subconductance transitions from and to closed channel. We then plotted these events cumulatively as a function of event number. A perfect straight line (correlation coefficient = 1.0, dashed line) is expected if each and all of the subconductance transitions occur from and to an open chan-

Downloaded from http://rupress.org/jgp/article-pdf/147/5/375/1795506/jgp_201511499.pdf by guest on 07 February 2026

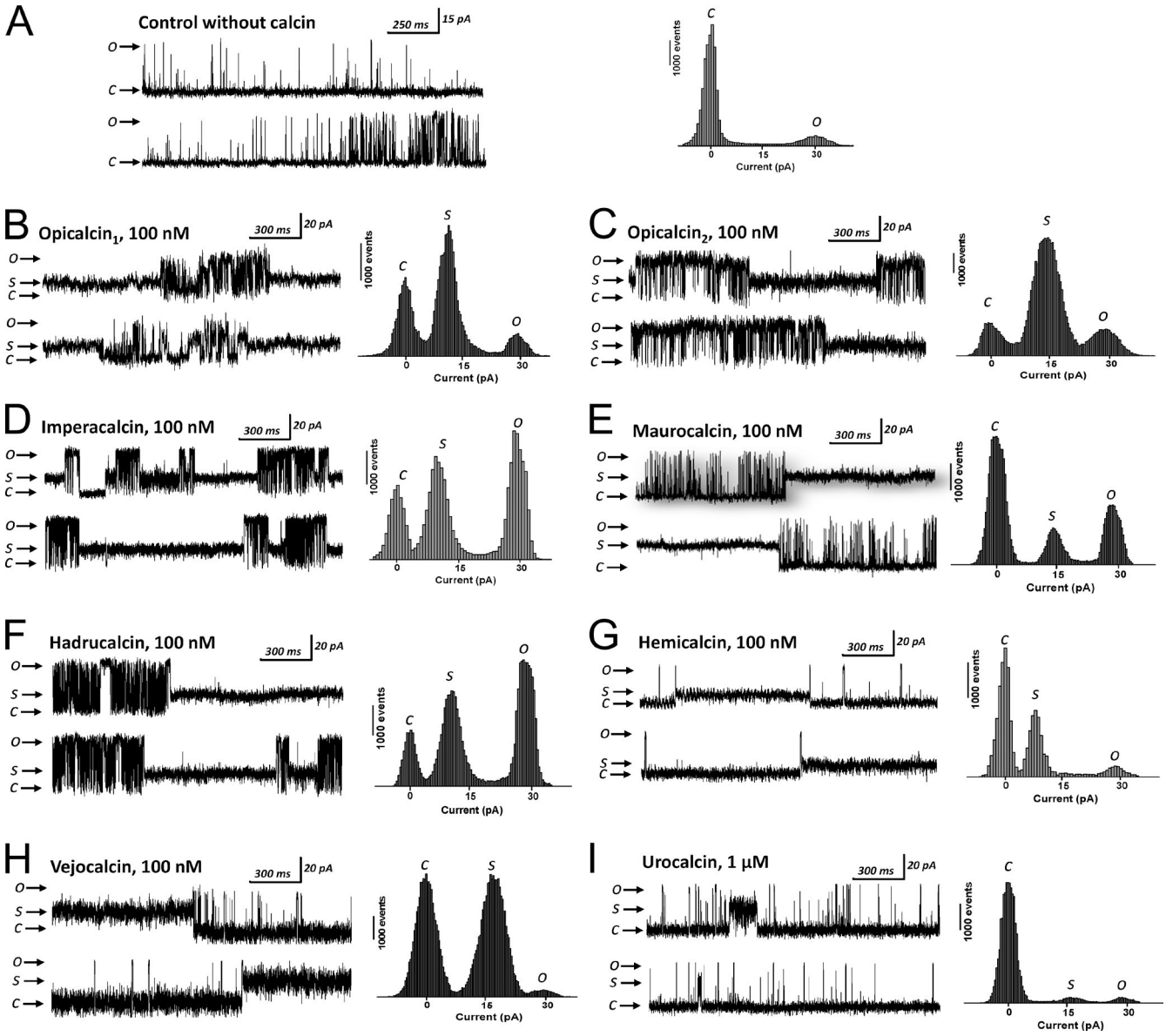

Figure 6. **Fractional subconductance value induced by calcins on single RyR1 channels.** RyR1 channel from rabbit skeletal muscle SR vesicles was reconstituted in lipid bilayers and recorded and analyzed as described in Materials and methods. (A) Single RyR1 channel in the absence of calcin is presented as control. (B–I) The eight calcins were added separately into the cis (cytosolic) chamber at the indicated concentration. *c* represents the zero current level when the channel is in the fully closed state, whereas *s* and *o* display the subconductance state and full opening of the channel, respectively. Current histograms from 10,000–30,000-ms segments of channel activity are shown at the right side of the traces for each calcin. The number of experiments varied for each calcin. Imperacalcin, maurocalcin, and hadrucalcin: n = 12, 8, and 5 different channels. All other calcins were tested at least two or three times.

nel, whereas a flat line with linear regression coefficient = 0 would be expected if none of the subconductance transitions occurs from and to open channel. Results (Fig. S2 D) clearly show that there is a strong dependence on a channel being open to initiate and terminate a calcin-induced substate. Most, but not all (open, on = 39/48 and open, off = 37/48), of the calcin-induced transitions occurred from and to open channel. An insufficient recording bandwidth may be a potential source of false negatives (missed open events before or after subconductance), and it is possible that the channel did open before or after subconductances, but the opening was so fast that we could not record it.

Ca^{2+} release from heavy SR

We also tested the capacity of calcins to induce Ca^{2+} release from rabbit skeletal heavy SR vesicles (Fig. 7). SR vesicles (1 µg/ml) were loaded with two consecutive additions of 50 µM Ca^{2+} followed by 25 µM Ca^{2+} thrice. Typically, each bolus addition of Ca^{2+} was actively taken up by the SR vesicles, and by the fifth bolus, extravesicular [Ca^{2+}] increased to ≈30 µM, indicating that the

Downloaded from http://rupress.org/jgp/article-pdf/147/5/375/1795506/jgp_201511499.pdf by guest on 07 February 2026

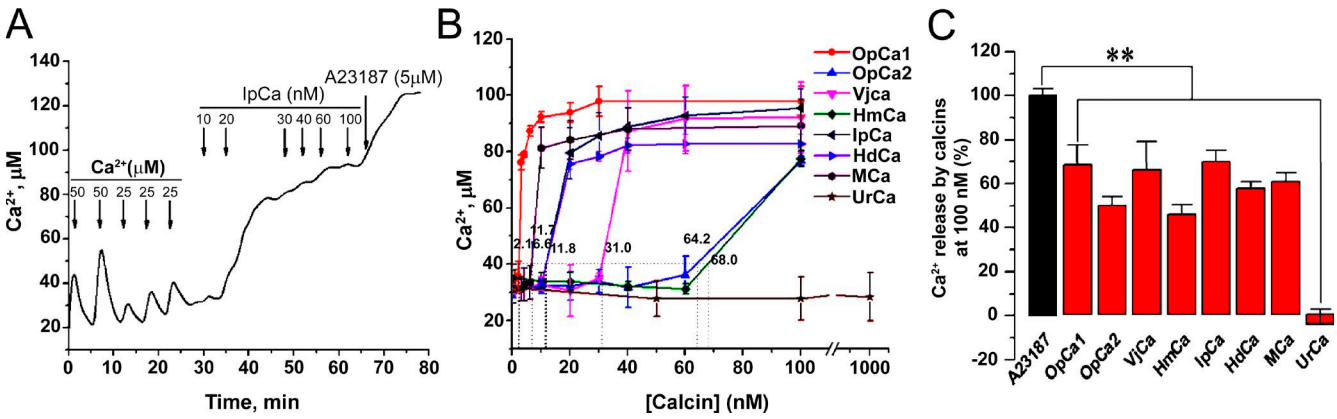

Figure 7. **Calcin-induced Ca^{2+} release from skeletal heavy SR vesicles.** (A) Typical trace of Ca^{2+} release by calcins. A concentration of 20 nM imperacalcin elicited abrupt Ca^{2+} release from SR vesicles, and further additions had incremental effects only. The fraction of calcin-induced Ca^{2+} release was calculated by adding the Ca^{2+} ionophore A23187 (5 μM). (B) Except urocalcin, all calcins elicited abrupt Ca^{2+} release within 100 nM (n = 3–4). (C) At 100 nM, all calcins except urocalcin elicited Ca^{2+} release to ~60% of total Ca^{2+} load from heavy SR. Mean ± SEM is shown. **, $P < 0.01$; calcins versus A23187, t test.

vesicles in the system were loaded to full capacity (Fig. 7 A). We then added each calcin and tested their ability to elicit Ca^{2+} release. Fig. 7 A shows a typical trace in which cumulative addition of imperacalcin elicits gradual Ca^{2+} release from SR vesicles. Addition of 10 nM imperacalcin produced initially modest Ca^{2+} release, but a second bolus that elevated imperacalcin to 20 nM elicited sharp Ca^{2+} release, and further imperacalcin additions yielded little additional release (Fig. 7 A). Addition of the Ca^{2+} ionophore A23187 (5 μM) to the reaction mixture indicated that imperacalcin released a fraction, only, of the total amount of Ca^{2+} trapped into the SR vesicles (≈70%; Fig. 7 C). Fig. 7 B show that this capacity of imperacalcin to release Ca^{2+} in a sharp, stepwise manner once a critical concentration has been reached, followed by incomplete emptying of the SR Ca^{2+} load at higher concentration, is a general property of all calcins (except urocalcin, see Fig. 7 C). Not surprisingly, the threshold for sharp Ca^{2+} release was the lowest for opicalcin$_1$ (2.1 ± 0.1 nM), followed by maurocalcin (6.6 ± 0.5 nM), imperacalcin (11.7 ± 0.6 nM), hadrucalcin (11.8 ± 0.4 nM), vejocalcin (31.0 ± 0.6 nM), opicalcin$_2$ (64.2 ± 5.5 nM), hemicalcin (68 ± 1.7 nM), and urocalcin (unable to release Ca^{2+} at concentration up to 1 μM). Thus, with the notable exception of opicalcin$_2$, calcins elicit Ca^{2+} release with roughly the same ranking order exhibited in [^{3}H]ryanodine binding experiments. Fig. 7 C shows that the total Ca^{2+} released by 100 nM calcin varied between 45% (hemicalcin) and 67% (opicalcin$_1$).

DISCUSSION

In this study, we present all native calcins known to date, including one novel (vejocalcin) and three previously uncharacterized (opicalcin$_1$, opicalcin$_2$, and urocalcin) peptides, and make a systematic, side by side comparison of their structural and functional attributes using an array of experimental ([^{3}H]ryanodine binding, Ca^{2+} release, and single RyR1 channel) assays, as well as bioinformatics analysis and three-dimensional modeling. Calcins are a relatively novel family of small (~3.7–4.2 kD), highly basic (pI = 9.3–10.1), compact peptides from scorpion venoms that target RyRs with high affinity and exquisite selectivity (no other targets known to date). Their remarkable stability is due to the fact that they fold along an evolutionarily conserved structural motif consisting of a triple-stranded, antiparallel β sheet stabilized by a ring formed of three disulfide bonds, known as an ICK motif. The ICK motif has been found in snail and spider toxins blockers of Ca^{2+} channels (Zhu et al., 2003), but not in other classes of scorpion toxins known to date (Na^+ channel modifiers, K^+ channel blockers, antimicrobial peptides, defensins), underscoring the unique arrangement of calcins among scorpion peptides. Primary sequence alignment and evolutionary analysis show a very close relationship among calcins, yet their natural variability yields peptides with binding affinity spanning ≈3 orders of magnitude, highlighting the importance of discrete domains in their interaction with RyR1 channels. We also show that the defining functional characteristic of all calcins is their capacity to stabilize RyR1 openings in a long-lasting subconducting state. This effect is nearly analogous to that of ryanodine, but unlike ryanodine, calcins rapidly bind to RyR1 channels and freely dissociate from their binding site (reversible effect), displaying a dose- and sequence-variable effect. Finally, although not assessed in this study, others (Estève et al., 2005; Boisseau et al., 2006) and we (Schwartz et al., 2009; Gurrola et al., 2010) have shown that, despite their highly ionized nature, calcins may penetrate cellular membranes, reach their intended target, and elicit

Downloaded from http://rupress.org/jgp/article-pdf/147/5/375/1795506/jgp_201511499.pdf by guest on 07 February 2026

Ca^{2+} release with several degrees of potency. Thus, this is a comprehensive study of calcins as a group of RyR-specific, cell-penetrating peptides (CPPs) that mobilize Ca^{2+} from intracellular stores with high dynamic range.

Ryanodine and calcins may bind independently and simultaneously to RyRs

It is well established that ryanodine binds to a conformationally sensitive (open) state of the RyR, so that the simplified Scheme 1, where C is closed, O is open, and O·Ry is the ryanodine-bound and subconducting state of the RyR, correctly describes the main kinetic steps of the reaction. A pertinent question here, however, is whether [^{3}H]ryanodine may properly monitor the binding of calcins given that they appear to bind to the same binding site in the RyR because of their highly similar effect. Ryanodine and calcins do bind to independent and nonoverlapping binding sites in the RyR, as indicated by the fact that addition of imperacalcin to ryanodine-modified RyR produces a calcin-induced substate of the ryanodine-modified substate (Tripathy et al., 1998), and hence, [^{3}H]ryanodine may suitably report the binding of calcin.

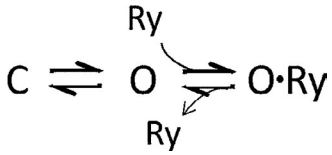

(Scheme 1)

By using in our assays a concentration of [^{3}H]ryanodine (7 nM) close to the K_d of the RyR–Ry complex at optimal [Ca^{2+}], we ensure that there is "room" for activators and inhibitors to exert their effect on the binding of [^{3}H]ryanodine. In principle, then, because [^{3}H]ryanodine binds at half of B_{max}, there should be approximately a twofold (100%) maximal increment of binding by a given agonist. Why, then, do calcins increase maximal binding to 300–500% above control? The most likely explanation is that they increase the "openness" of the channel above and beyond what Ca^{2+} alone is capable of doing. The calcin-induced substate of long duration promotes more effectively the binding of [^{3}H]ryanodine than the frequent but brief openings (flickering) induced by Ca^{2+} alone. Thus, by requiring an open channel to bind and simultaneously promoting opening of the channel, calcins increase the dynamic range of the [^{3}H]ryanodine binding assay, and the latter efficiently reports the binding of the calcins. Scheme 2, therefore, describes the binding of ryanodine (Ry) and calcin (Cn) to open RyR (O) in simplified terms, where O·Cn is the calcin-bound open RyR and O·Cn·Ry is the calcin- and ryanodine-bound open RyR. Because of the slow association rate of ryanodine to RyRs, transitions from O to doubly occupied O·Cn·Ry probably go through O·Cn first, but Scheme 2 depicts the complex at equilibrium. Simultaneous occupation and additive effects of ryanodine and calcins are thus possible, and our [^{3}H]ryanodine binding assays here suitably reported this combined interaction. However, a caveat is that by using [Ry] at a concentration equal to its K_d, we impose the equality $P(O) = P(O{\cdot}Ry)$ (where $P(O)$ and $P(O{\cdot}Ry)$ are occupancies or probabilities of the corresponding states). Thus, the value of bound Ry relative to a well-determined B_{max} should then be a direct measure of $P(O)$. This could be different from the probability of opening as observed in reconstituted RyR channels and constitutes a limitation of our binding approach.

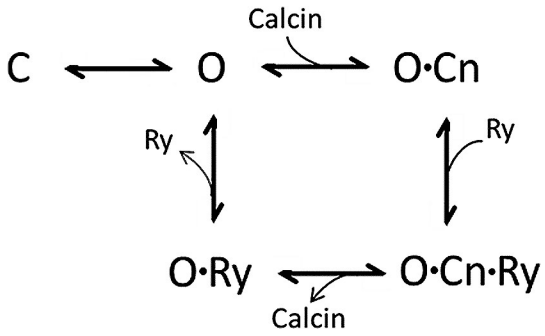

(Scheme 2)

Primary sequence and natural variations

Previous studies have addressed the effect of artificial mutations on calcins' properties, i.e., alanine scanning on imperacalcin (Lee et al., 2004) and selected monosubstitutions on maurocalcin (Mabrouk et al., 2007). Here we examined nature's own experimentation that includes subtle (and others seemingly drastic) mono-, di-, and multi-variations from an apparently common pattern of design. Comparison of calcins' primary sequence permitted discernment of some of their most salient structural attributes and unique domains among scorpion peptides (Fig. 2). First, six highly conserved cysteines serve as the framework to flawlessly align calcins, with an identical number of amino acids interspaced between cysteines (no need to introduce gaps or delete residues to maximize homology). ^{1}H-NMR of maurocalcin (Mosbah et al., 2000) and imperacalcin (Lee et al., 2004) confirmed that these cysteines are oxidized in the mature peptide and form disulfide bonds with the precise pairing Cys^3-Cys^{17}, Cys^{10}-Cys^{21}, and Cys^{16}-Cys^{32}. Maintenance of this disulfide-bonded core is essential not only to support the ICK motif, the signature folding of this family of scorpion peptides, but improperly paired or linear (disulfide-less) peptides are pharmacologically inert (Zamudio et al., 1997; Lee et al., 2004; Ram et al., 2008), indicating that the disulfide bonds buttress the tertiary structure that forms the cal-

Downloaded from http://rupress.org/jgp/article-pdf/147/5/375/1795506/jgp_201511499.pdf by guest on 07 February 2026

cins' active site. Second, an abundance of basic amino acids is another remarkable feature of calcins (Figs. 2 A and 4). All peptides in this group are composed of at least 27% (vejocalcin) and as much as 39% (urocalcin) of positively charged amino acids. In the linear sequence, these basic residues (bolded) appear in three main clusters, namely, ^{8}KRCR^{11} (cluster 1), ^{19}KKCKRR^{24} (cluster 2), and ^{30}KRCR^{33} (cluster 3). Notice how cysteines (C) "break" the continuity of basic residues in the clusters, perhaps not fortuitously, because the disulfide bonds that they form will "pull" together these residues in the tertiary structure (Fig. S1), contributing to expand even more the size of the clusters.

Except for relatively rare exceptions, clusters 2 and 3 are remarkably conserved, stressing the prominent hierarchy of these motifs, whereas cluster 1 is interrupted by Leu or Gln in five out of eight calcins, also suggesting a lesser structural rank for this cluster. Indeed, in the first mutational study performed on calcins, we found that the mutation R23E, at the heart of cluster 2, completely abolished the capacity of imperacalcin to stimulate [^{3}H]ryanodine binding and Ca^{2+} release and to induce subconductance states in RyR1 (Gurrola et al., 1999), an effect that was also observed with an even milder mutation (R23A) in imperacalcin (Lee et al., 2004) and maurocalcin (Chen et al., 2003; Lukács et al., 2008). In contrast, mutation K8E in imperacalcin had only modest effects (Gurrola et al., 1999), supporting the notion that cluster 1 plays a lesser role in the calcin–RyR1 interaction. Gurrola et al. (1999) also proposed that cluster 2 in extension to Thr26 (^{19}KKCKRRGT^{26}) was structurally similar to a segment of peptide A of the α1 subunit of the DHPR1 that was presumed to interact directly with RyR1 in the excitation–contraction coupling of skeletal muscle (Saiki et al., 1999) and showed that the mutation T26A decreased the affinity of imperacalcin by 10-fold. Although the participation of peptide A in excitation–contraction coupling is debated today, several studies have found a mechanism of activation of RyR1 that is common to peptide A and calcins (specifically, imperacalcin [Dulhunty et al., 2004] and maurocalcin [Chen et al., 2003]), again underscoring the importance of cluster 2 as integral part of calcins' active site. The latter most likely encompasses Thr26 also, as in the present study we demonstrate that opicalcin$_1$ and opicalcin$_2$, which differ only by one amino acid (T26A), display a 10-fold difference in affinity. However, it is unlikely that the calcins' active site is wholly contained in cluster 2 and Thr26, as the three-dimensional model of calcins clearly shows that cluster 3 intertwines with cluster 2 to form a "mega-cluster" of basic residues that crowds the lower end of the frontal face of calcins and is largely responsible for its highly positive charge (Fig. 4). In support of cluster 3 participation in the calcin–RyR1 interaction, Ala substitutions of K30, R31, and R33 drastically decreased the affinity of imperacalcin for RyR1 (from 28 to >1,000,000 nM [Dulhunty et al., 2004]). Again, in sharp contrast, cluster 1 residues populate the upper end of the molecule and are more prominent on the flank of the dorsal face (Fig. 4), apparently far from the residues of clusters 2 and 3 whose substitution dramatically decreases the affinity of calcins. Overall, then, clusters 2 and 3 appear of primordial importance for calcin interaction with RyRs by means of their coalescing into a single mega-cluster of positive charges in one face of the peptide. Because electrostatic interactions govern the calcin–RyR1 interaction (Tripathy et al., 1998), it is likely that this mega-cluster forms a cloud of positive charges that interacts with negatively charged residues in RyRs.

Thus, in general terms, the calcin sequence can be roughly split in half to yield a highly variable N-terminal segment (^{1}G-N^{14}) and a remarkably conserved C-terminal segment (^{15}D-R^{33}). Previous studies on imperacalcin (Lee et al., 2004) and maurocalcin (Mabrouk et al., 2007) have shown that, as a general rule of thumb, mutations affecting positively charged residues dramatically decrease or even abolish [^{3}H]ryanodine binding, whereas mutations affecting negatively charged residues slightly increase the affinity of these calcins. Mutations of neutral residues can increase, decrease, or have no significant effect (Lee et al., 2004; Mabrouk et al., 2007). However, examination of the array of calcins presented here reveals more nuances and complexity in this general rule. For example, let's compare the primary sequences of opicalcin$_1$ and urocalcin (Fig. 2), the calcins with the highest (~0.3 nM) and the lowest (~300 nM) affinity for RyR1 (Fig. 5), to attempt rationalization of their wildly diverse pharmacological potency. Urocalcin presents the natural substitutions R9L (cluster 1) and K20S (cluster 2), which according to the general rule and our discussion above should separately have modest and major effects, respectively, on binding affinity, and their combined presence might explain the drastic reduction of urocalcin's affinity. However, similar substitutions are present in vejocalcin (R9L in cluster 1 and K22S in cluster 2), and yet its K_d is 3.7 ± 0.4 nM, which is as high as that of opicalcin$_2$. In fact, a third substitution in cluster 3 (K30Q) should theoretically decrease the affinity of vejocalcin even more than that of urocalcin. Obviously, simply following the rule of thumb will not predict the degree of affinity change brought about by a set of mutations, even if they occur at domains that are presumably part of the active site. Instead, it seems that a more comprehensive approach must be followed to ascertain the role of substitutions that appear innocuous in the calcins' landscape. What is peculiar about urocalcin (compared with opicalcin$_1$) is not only the substitutions of critical residues in clusters 1 and 2 but also the presence of four additional basic residues in the N-terminal half of the molecule (Fig. 2). Intuitively, these extra positive charges should have resulted in a superior calcin following the rule of thumb, but analysis of their three-dimen-

Downloaded from http://rupress.org/jgp/article-pdf/147/5/375/1795506/jgp_201511499.pdf by guest on 07 February 2026

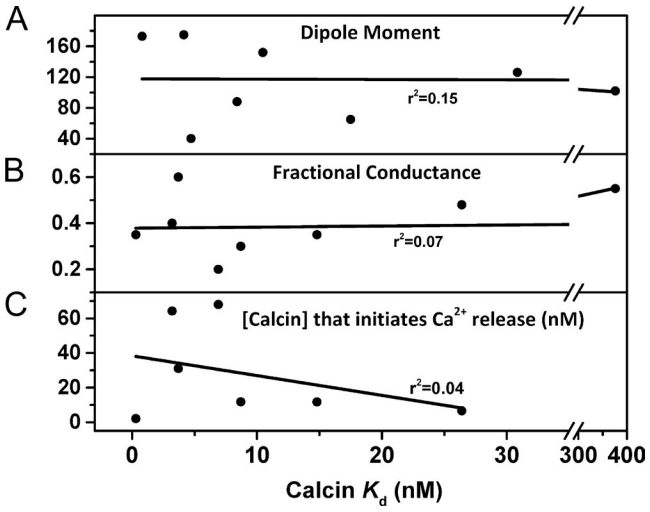

Figure 8. **DM, fractional conductance, and Ca^{2+} release appear unrelated to the K_d of calcins.** (A) Plot of DM versus K_d of [^{3}H]ryanodine binding. The DMs have a poor correlation with the binding affinity (r^2 = 0.15). (B) Subconductance versus K_d of [^{3}H]ryanodine binding. The position of subconductance induced by calcin is unrelated to the K_d of [^{3}H]ryanodine binding (r^2 = 0.07). (C) Ca^{2+} release versus [^{3}H]ryanodine binding. No correlation is seen between calcin concentration that induces Ca^{2+} release and K_d of [^{3}H]ryanodine binding (r^2 = 0.04).

sional arrangement (Fig. 4 G) shows that they all protrude in the upper end of the frontal side of the molecule and intertwine with hydrophobic residues to dissipate a hydrophobic core that dominates this part of most calcins. Hence, an integral approach that considers variations in domains established to play primordial roles in receptor recognition (clusters 2 and 3) plus evaluation of the calcin's overall amphipathicity (integrity of its hydrophobic and hydrophilic cores) are among the structural features that should be considered in the rational design of competent calcins.

DM of calcins

In addition to the signature ICK motif folding promoted by the three highly conserved disulfide bridges, a marked anisotropy of electrostatic charge distribution, where most of the positively charged residues are segregated in one end of the molecule, appears as a prevalent feature in the calcin family of peptides. This coalescence of basic residues presents a large functional surface area to interact with the RyRs (Mosbah et al., 2000; Lee et al., 2004) and generates a discrete DM. In principle, DM could be related to binding affinity because a larger DM could imply larger surface area to interact with RyRs, but other possibilities could undermine this relationship. In this study, we found that opicalcin$_1$, opicalcin$_2$, and imperacalcin have similar DM values, but the affinity of opicalcin$_1$ is 10.7-fold and 29-fold higher than that of opicalcin$_2$ and imperacalcin, respectively. Also, vejocalcin, which lacks the positively charged residues K22 and K30 (K22S and K30Q, instead) in the predicted functional face of calcins, has the smallest DM (40 D) but similar activity as opicalcin$_2$, which presents the largest DM (175 D). Hadrucalcin, whose relatively small DM (65 D) is mainly the result of an increase of positively charged residues in the nonfunctional face, still has strong affinity for RyR1 (14.8 ± 1.9 nM), whereas urocalcin, which also scatters its positively charged residues to the upper end of the frontal face of the molecule and thus decreases its DM value (102 D), has the weakest affinity for RyR1 (376 ± 45 nM), over 1,000-fold lower than that of opicalcin$_1$ and 25-fold lower than that of hadrucalcin. Thus, there appears to be no correlation between DM and affinity, and a plot of DM values versus K_d (as determined in [^{3}H]ryanodine binding assays) yields a correlation coefficient r^2 = 0.15 (Fig. 8 A), indicating that DMs or electrical amphiphilicity is not associated with the interaction with RyRs. In support of this conclusion, D-maurocalcin, a chiral analogue of maurocalcin composed of D–amino acids (instead of L–amino acids) that has identical charge distribution as the parent maurocalcin, completely loses the ability to stimulate [^{3}H]ryanodine binding and Ca^{2+} release (Poillot et al., 2010). Thus, simply characterizing the calcins by charge anisotropy or electrical amphiphilicity is insufficient to formulate a model of calcin–RyR1 interaction, and the spatial conformation of calcins also plays as critical a role as the aggregation of positively charged residues in the calcin–RyR interacting process.

Single channel effect and mechanism

Several calcins have been tested on single RyRs, but a mechanistic understanding of their common biophysical effect has been mainly derived from experiments with imperacalcin (Tripathy et al., 1998) and maurocalcin (Lukács et al., 2008). When added to the cytosolic side of the channel, imperacalcin induces voltage- and concentration-dependent subconductance states in both skeletal and cardiac RyRs. Analysis of voltage and concentration dependence and kinetics of substate formation suggests that induction of subconductance states corresponds to reversible, voltage-dependent binding and unbinding of imperacalcin at a single site located at ∼23% of the voltage drop from the cytosolic side (Tripathy et al., 1998). The mechanism of substate formation by imperacalcin is not entirely clear, but several scenarios are applicable to calcins in general: steric mechanisms (i.e., calcin binding to residues within the ion conduction pathway to restrict ion flow), allosteric mechanisms (i.e., calcin binding to a site distant to the conduction pathway and altering the shape or charge of the RyR's conduction pathway), and a combination thereof. However, because imperacalcin accesses its binding site by entering the channel through a cytosolically accessible opening (Tripathy et al., 1998), we favor a mechanism whereby calcin reaches its binding site located in the SR membrane–adjacent ion conduction pathway by entering the channel through a vesti-

Downloaded from http://rupress.org/jgp/article-pdf/147/5/375/1795506/jgp_201511499.pdf by guest on 07 February 2026

bule's pore with a diameter ≥2.5 nm (the diameter of globular imperacalcin). Our data do not allow us to discard any of the mechanisms above, but interestingly, recent near-atomic resolution of the three-dimensional structure of RyR1 reveals an opening of ∼5 nm in the center of the channel, most precisely in the convergence of the N-terminal domains that form part of the most external layer of the channel facing the t-tubules (Efremov et al., 2015; Yan et al., 2015; Zalk et al., 2015), thus evidencing the existence of a wide vestibule in the cytosolic side of the RyR1. Accordingly, we favor the notion that globular calcins, all with surface diameter ≤3 nm, induce their characteristic subconductance state by entering the channel through this cytosolic opening and accessing their binding site deep in the core of the channel. This possibility needs to be tested experimentally.

In an alternative scenario, Samsó et al. (1999), using cryo-electron microscopy and three-dimensional single-particle image analysis, found that imperacalcin binds to a cytoplasmic crevice in each RyR1 subunit (four binding sites/channel tetramer) located near the calmodulin-binding site and far (<11 nm) from the center of the transmembrane region of the channel (Samsó et al., 1999), supporting an allosteric mechanism of action of imperacalcin as opposed to the mechanism of direct positioning of the peptide within the ion conduction pathway. It is worth noting, however, that the cryo-electron microscopy experiments of Samsó et al. (1999) required imperacalcin covalently bound to biotin, which subsequently bound to streptavidin-coated gold particles to facilitate localization of this ligand in single channel images and that these additional tags increased the surface area of imperacalcin, probably beyond the maximum allowed to enter the vestibule of the channel and reach the binding site described above. In other words, the imperacalcin–biotin–streptavidin complex could have been too bulky to have accessed the binding site within the ion conduction pathway that we believe induces the signature subconductance state.

Instead, we favor the notion that imperacalcin–biotin–streptavidin likely bound to a secondary and external binding site (the crevice described in the previous paragraph) that is also accessed by peptide A (Gurrola et al., 1999; Chen et al., 2003; Dulhunty et al., 2004; Altafaj et al., 2005). Only by binding to external sites of the RyR1 (one for each monomer) does the idea that imperacalcin and peptide A mimic a segment of the DHPR1 that interacts with the RyR1 during e-c coupling appear to make sense. In this scenario, occupancy of these external binding sites could activate the RyR1, but induction of the characteristic subconductance state described here appears unlikely because the latter follows the rules of a bimolecular reaction (one calcin–one channel) and requires proximity to the SR-adjacent voltage drop of the channel (Tripathy et al., 1998).

Regardless of their precise mechanism of action, the reversible, concentration- and voltage-dependent, long-lasting subconductance state constitutes the signature effect of calcins on RyRs, and this substate has been measured up to now for imperacalcin (Tripathy et al., 1998; Gurrola et al., 1999), maurocalcin (Fajloun et al., 2000; Chen et al., 2003), hemicalcin (Shahbazzadeh et al., 2007), and hadrucalcin (Schwartz et al., 2009), with fractional values of the full conductance state corresponding to 0.35, 0.48, 0.38, and 0.35, respectively. Here we report for the first time the fractional conductance induced by the remaining four calcins opicalcin$_1$ (0.35), opicalcin$_2$ (0.40), vejocalcin (0.60), and urocalcin (0.55; Fig. 5). Furthermore, in our experiments, the subconductance induced by hemicalcin was only 0.2 of full conductance, lower than that reported previously (Shahbazzadeh et al., 2007) and most likely caused by the rectifying conductance induced by the calcin (i.e., the proportion of the substate is lower at higher positive voltages [Tripathy et al., 1998]). Considering the high structural similarity among calcins, it is likely that they bind to RyR1 at the same site but engage the receptive amino acids with varying degrees of affinity because of the charge distribution and structural conformation that is unique to each calcin. An interesting example is urocalcin, whose subconductance is induced only at the cumulative dose of 1 µM or higher, with low frequency and short duration (<500 ms), indicating that urocalcin loosely associates to, and readily dissociates from, the calcin site in RyR1 (Fig. 6). We also correlated the subconductance value with the binding activity and the ability to stimulate Ca^{2+} release; however, no relationship is seen (Fig. 8 B), suggesting that the capacity of calcins to stimulate [^{3}H]ryanodine binding and Ca^{2+} release may be associated with the dwell time of the calcin in the RyR1 (mean duration of subconductance) rather than the fractional value of the substate, but more experiments are needed to confirm this.

Ca^{2+} release from heavy SR

Calcins induce Ca^{2+} release at concentrations that are crudely correlated with their [^{3}H]ryanodine binding affinity, with opicalcin$_1$ and urocalcin displaying the strongest and weakest capacity, respectively, to stimulate both [^{3}H] ryanodine binding and Ca^{2+} release. But the correlation is not perfect for most calcins in between; for example, hemicalcin and maurocalcin show deviations in correlation, and opicalcin$_2$ displays strong binding affinity but weaker ability to stimulate Ca^{2+} release (Fig. 8 C). This may be explained by the fact that Ca^{2+}-induced Ca^{2+} release (CICR) is a nonlinear process, with inherent self-reinforcing features and sensitive to total SR Ca^{2+} load (Stern and Cheng, 2004). Hence, once a calcin "traps" a critical number of RyRs in its specific subconducting state (a step dependent on calcin affinity), it will induce Ca^{2+} release that in turn will induce more Ca^{2+} release (a step independent of calcin affinity). Thus, the calcin-induced fractional Ca^{2+} release (Ca^{2+} released/total SR Ca^{2+} content) will depend

Downloaded from http://rupress.org/jgp/article-pdf/147/5/375/1795506/jgp_201511499.pdf by guest on 07 February 2026

not only on the affinity of calcins for RyRs, but also in the self-amplifying nature of CICR and the amount of Ca^{2+} load in the SR. Although the relationship affinity-fractional Ca^{2+} release held as expected for the highest and weakest calcin, the assay was not sensitive enough to discriminate flawlessly for calcins of medium affinity. An interesting phenomenon that is not seen with other agonists of RyRs (i.e., caffeine or 4-chloro-m-cresol) is that calcin-induced Ca^{2+} release will consistently be a fraction of the total SR Ca^{2+} load; that is, a residual amount of Ca^{2+} will remain in the SR vesicles even at saturating calcin concentration (Fig. 7). The mechanism underlying this phenomenon is unclear but might be related to the property of calcins to induce a partial rather than a complete opening of RyRs, so that even when all RyRs are calcin-occupied, the total Ca^{2+} flow out of the SR is limited by the subconducting value and may be in balance with Ca^{2+} reuptake by the Ca^{2+} pump.

Summary

In summary, we have characterized by several functional assays the most salient structural features of all calcins known to date. Natural variations in amino acid sequence endow these peptides with a range of RyR affinity that spans ∼3 orders of magnitude and variable capacity to stimulate [^{3}H]ryanodine binding and Ca^{2+} release. Despite their variations in amino acid sequence, all calcins fold along an ICK motif that maintains a globular and highly compact structure. The relatively small surface area of calcins suggests that their structure is already minimized, with all residues contributing at least partly to RyR1 binding and/or membrane permeation. Still, analysis of natural calcin variations recognizes prominent roles for discrete structural domains, with two clusters of basic residues in the carboxyl end (^{19}KKCKRR^{24} and ^{30}KRCR^{33}) appearing essential for RyR1 pharmacology. At the single RyR1 channel level, calcins, unlike the effect of ryanodine, induce the appearance of a long-lasting but reversible subconductance state. This subconductance state is dose dependent and varies in amplitude for each calcin. Thus, the calcin family of peptides offers a diversified set of RyR ligands with the capacity to modulate RyRs in situ and with high dynamic range and potency.

ACKNOWLEDGMENTS

We are grateful to reviewer 1 for suggesting a potential mechanism of interaction of calcin with the RyR.

This study was supported by National Institutes of Health grants R01-HL120108 and R01-HL055438 (to H.H. Valdivia) and Dirección General Asuntos del Personal Académico, Universidad Nacional Autónoma de México (DGAP, UNAM) grant IN200113 (to L.D. Possani).

The authors declare no competing financial interests.

Eduardo Ríos served as editor.

Submitted: 14 August 2015
Accepted: 21 March 2016

REFERENCES

Abramson, J.J., E. Buck, G. Salama, J.E. Casida, and I.N. Pessah. 1988. Mechanism of anthraquinone-induced calcium release from skeletal muscle sarcoplasmic reticulum. *J. Biol. Chem.* 263:18750–18758.

Altafaj, X., W. Cheng, E. Estève, J. Urbani, D. Grunwald, J.M. Sabatier, R. Coronado, M. De Waard, and M. Ronjat. 2005. Maurocalcine and domain A of the II-III loop of the dihydropyridine receptor Cav 1.1 subunit share common binding sites on the skeletal ryanodine receptor. *J. Biol. Chem.* 280:4013–4016. http://dx.doi.org/10.1074/jbc.C400433200

Ather, S., J.L. Respress, N. Li, and X.H. Wehrens. 2013. Alterations in ryanodine receptors and related proteins in heart failure. *Biochim. Biophys. Acta.* 1832:2425–2431. http://dx.doi.org/10.1016/j.bbadis.2013.06.008

Benkusky, N.A., E.F. Farrell, and H.H. Valdivia. 2004. Ryanodine receptor channelopathies. *Biochem. Biophys. Res. Commun.* 322:1280–1285. http://dx.doi.org/10.1016/j.bbrc.2004.08.033

Bers, D.M. 2002. Cardiac excitation-contraction coupling. *Nature.* 415:198–205. http://dx.doi.org/10.1038/415198a

Bers, D.M. 2004. Macromolecular complexes regulating cardiac ryanodine receptor function. *J. Mol. Cell. Cardiol.* 37:417–429. http://dx.doi.org/10.1016/j.yjmcc.2004.05.026

Boisseau, S., K. Mabrouk, N. Ram, N. Garmy, V. Collin, A. Tadmouri, M. Mikati, J.M. Sabatier, M. Ronjat, J. Fantini, and M. De Waard. 2006. Cell penetration properties of maurocalcine, a natural venom peptide active on the intracellular ryanodine receptor. *Biochim. Biophys. Acta.* 1758:308–319. http://dx.doi.org/10.1016/j.bbamem.2006.02.007

Chen, L., E. Estève, J.M. Sabatier, M. Ronjat, M. De Waard, P.D. Allen, and I.N. Pessah. 2003. Maurocalcine and peptide A stabilize distinct subconductance states of ryanodine receptor type 1, revealing a proportional gating mechanism. *J. Biol. Chem.* 278:16095–16106. http://dx.doi.org/10.1074/jbc.M209501200

Curran, J., M.J. Hinton, E. Ríos, D.M. Bers, and T.R. Shannon. 2007. β-Adrenergic enhancement of sarcoplasmic reticulum calcium leak in cardiac myocytes is mediated by calcium/calmodulin-dependent protein kinase. *Circ. Res.* 100:391–398. http://dx.doi.org/10.1161/01.RES.0000258172.74570.e6

Dulhunty, A.F., S.M. Curtis, S. Watson, L. Cengia, and M.G. Casarotto. 2004. Multiple actions of imperatoxin A on ryanodine receptors: interactions with the II-III loop "A" fragment. *J. Biol. Chem.* 279:11853–11862. http://dx.doi.org/10.1074/jbc.M310466200

Dyck, J.D., T.E. David, B. Burke, G.D. Webb, M.A. Henderson, and R.S. Fowler. 1987. Management of coronary artery disease in Hutchinson-Gilford syndrome. *J. Pediatr.* 111:407–410. http://dx.doi.org/10.1016/S0022-3476(87)80466-3

Efremov, R.G., A. Leitner, R. Aebersold, and S. Raunser. 2015. Architecture and conformational switch mechanism of the ryanodine receptor. *Nature.* 517:39–43. http://dx.doi.org/10.1038/nature13916

El-Hayek, R., A.J. Lokuta, C. Arévalo, and H.H. Valdivia. 1995. Peptide probe of ryanodine receptor function. Imperatoxin A, a peptide from the venom of the scorpion *Pandinus imperator*, selectively activates skeletal-type ryanodine receptor isoforms. *J. Biol. Chem.* 270:28696–28704. http://dx.doi.org/10.1074/jbc.270.48.28696

Estève, E., K. Mabrouk, A. Dupuis, S. Smida-Rezgui, X. Altafaj, D. Grunwald, J.C. Platel, N. Andreotti, I. Marty, J.M. Sabatier, et al. 2005. Transduction of the scorpion toxin maurocalcine into cells. Evidence that the toxin crosses the plasma membrane. *J. Biol. Chem.* 280:12833–12839. http://dx.doi.org/10.1074/jbc.M412521200

Fajloun, Z., R. Kharrat, L. Chen, C. Lecomte, E. Di Luccio, D. Bichet, M. El Ayeb, H. Rochat, P.D. Allen, I.N. Pessah, et al.

Downloaded from http://rupress.org/jgp/article-pdf/147/5/375/1795506/jgp_201511499.pdf by guest on 07 February 2026

2000. Chemical synthesis and characterization of maurocalcine, a scorpion toxin that activates Ca^{2+} release channel/ryanodine receptors. *FEBS Lett.* 469:179–185. http://dx.doi.org/10.1016/S0014-5793(00)01239-4

Fill, M., and J.A. Copello. 2002. Ryanodine receptor calcium release channels. *Physiol. Rev.* 82:893–922. http://dx.doi.org/10.1152/physrev.00013.2002

Gurrola, G.B., C. Arévalo, R. Sreekumar, A.J. Lokuta, J.W. Walker, and H.H. Valdivia. 1999. Activation of ryanodine receptors by imperatoxin A and a peptide segment of the II-III loop of the dihydropyridine receptor. *J. Biol. Chem.* 274:7879–7886. http://dx.doi.org/10.1074/jbc.274.12.7879

Gurrola, G.B., E.M. Capes, F.Z. Zamudio, L.D. Possani, and H.H. Valdivia. 2010. Imperatoxin A, a cell-penetrating peptide from scorpion venom, as a probe of Ca-release channels/ryanodine receptors. *Pharmaceuticals (Basel).* 3:1093–1107. http://dx.doi.org/10.3390/ph3041093

Hakamata, Y., J. Nakai, H. Takeshima, and K. Imoto. 1992. Primary structure and distribution of a novel ryanodine receptor/calcium release channel from rabbit brain. *FEBS Lett.* 312:229–235. http://dx.doi.org/10.1016/0014-5793(92)80941-9

Kong, H., P.P. Jones, A. Koop, L. Zhang, H.J. Duff, and S.R. Chen. 2008. Caffeine induces Ca^{2+} release by reducing the threshold for luminal Ca^{2+} activation of the ryanodine receptor. *Biochem. J.* 414:441–452. http://dx.doi.org/10.1042/BJ20080489

Kumar, S. 1996. A stepwise algorithm for finding minimum evolution trees. *Mol. Biol. Evol.* 13:584–593. http://dx.doi.org/10.1093/oxfordjournals.molbev.a025618

Lai, F.A., H.P. Erickson, E. Rousseau, Q.Y. Liu, and G. Meissner. 1988. Purification and reconstitution of the calcium release channel from skeletal muscle. *Nature.* 331:315–319. http://dx.doi.org/10.1038/331315a0

Lee, C.W., E.H. Lee, K. Takeuchi, H. Takahashi, I. Shimada, K. Sato, S.Y. Shin, D.H. Kim, and J.I. Kim. 2004. Molecular basis of the high-affinity activation of type 1 ryanodine receptors by imperatoxin A. *Biochem. J.* 377:385–394. http://dx.doi.org/10.1042/bj20031192

Lukács, B., M. Sztretye, J. Almássy, S. Sárközi, B. Dienes, K. Mabrouk, C. Simut, L. Szabó, P. Szentesi, M. De Waard, et al. 2008. Charged surface area of maurocalcine determines its interaction with the skeletal ryanodine receptor. *Biophys. J.* 95:3497–3509. http://dx.doi.org/10.1529/biophysj.107.120840

Lukyanenko, V., I. Györke, S. Subramanian, A. Smirnov, T.F. Wiesner, and S. Györke. 2000. Inhibition of Ca^{2+} sparks by ruthenium red in permeabilized rat ventricular myocytes. *Biophys. J.* 79:1273–1284. http://dx.doi.org/10.1016/S0006-3495(00)76381-8

Luna-Ramírez, K., V. Quintero-Hernández, L. Vargas-Jaimes, C.V. Batista, K.D. Winkel, and L.D. Possani. 2013. Characterization of the venom from the Australian scorpion *Urodacus yaschenkoi*: Molecular mass analysis of components, cDNA sequences and peptides with antimicrobial activity. *Toxicon.* 63:44–54. http://dx.doi.org/10.1016/j.toxicon.2012.11.017

Mabrouk, K., N. Ram, S. Boisseau, F. Strappazzon, A. Rehaim, R. Sadoul, H. Darbon, M. Ronjat, and M. De Waard. 2007. Critical amino acid residues of maurocalcine involved in pharmacology, lipid interaction and cell penetration. *Biochim. Biophys. Acta.* 1768:2528–2540. http://dx.doi.org/10.1016/j.bbamem.2007.06.030

Meissner, G. 1984. Adenine nucleotide stimulation of Ca^{2+}-induced Ca^{2+} release in sarcoplasmic reticulum. *J. Biol. Chem.* 259:2365–2374.

Mosbah, A., R. Kharrat, Z. Fajloun, J.G. Renisio, E. Blanc, J.M. Sabatier, M. El Ayeb, and H. Darbon. 2000. A new fold in the scorpion toxin family, associated with an activity on a ryanodine-sensitive calcium channel. *Proteins.* 40:436–442. http://dx.doi.org/10.1002/1097-0134(20000815)40:3<436::AID-PROT90>3.0.CO;2-9

Nabhani, T., X. Zhu, I. Simeoni, V. Sorrentino, H.H. Valdivia, and J. García. 2002. Imperatoxin a enhances Ca^{2+} release in developing skeletal muscle containing ryanodine receptor type 3. *Biophys. J.* 82:1319–1328. http://dx.doi.org/10.1016/S0006-3495(02)75487-8

Nakai, J., T. Imagawa, Y. Hakamat, M. Shigekawa, H. Takeshima, and S. Numa. 1990. Primary structure and functional expression from cDNA of the cardiac ryanodine receptor/calcium release channel. *FEBS Lett.* 271:169–177. http://dx.doi.org/10.1016/0014-5793(90)80399-4

Pessah, I.N., R.A. Stambuk, and J.E. Casida. 1987. Ca^{2+}-activated ryanodine binding: mechanisms of sensitivity and intensity modulation by Mg^{2+}, caffeine, and adenine nucleotides. *Mol. Pharmacol.* 31:232–238.

Poillot, C., K. Dridi, H. Bichraoui, J. Pêcher, S. Alphonse, B. Douzi, M. Ronjat, H. Darbon, and M. De Waard. 2010. D-Maurocalcine, a pharmacologically inert efficient cell-penetrating peptide analogue. *J. Biol. Chem.* 285:34168–34180. http://dx.doi.org/10.1074/jbc.M110.104919

Ram, N., N. Weiss, I. Texier-Nogues, S. Aroui, N. Andreotti, F. Pirollet, M. Ronjat, J.M. Sabatier, H. Darbon, V. Jacquemond, and M. De Waard. 2008. Design of a disulfide-less, pharmacologically inert, and chemically competent analog of maurocalcine for the efficient transport of impermeant compounds into cells. *J. Biol. Chem.* 283:27048–27056. http://dx.doi.org/10.1074/jbc.M804727200

Rosales, R.A., M. Fill, and A.L. Escobar. 2004. Calcium regulation of single ryanodine receptor channel gating analyzed using HMM/MCMC statistical methods. *J. Gen. Physiol.* 123:533–553. http://dx.doi.org/10.1085/jgp.200308868

Rousseau, E., and G. Meissner. 1989. Single cardiac sarcoplasmic reticulum Ca2+-release channel: activation by caffeine. *Am. J. Physiol.* 256:H328–H333.

Saiki, Y., R. El-Hayek, and N. Ikemoto. 1999. Involvement of the Glu724-Pro760 region of the dihydropyridine receptor II-III loop in skeletal muscle-type excitation-contraction coupling. *J. Biol. Chem.* 274:7825–7832. http://dx.doi.org/10.1074/jbc.274.12.7825

Samsó, M., R. Trujillo, G.B. Gurrola, H.H. Valdivia, and T. Wagenknecht. 1999. Three-dimensional location of the imperatoxin A binding site on the ryanodine receptor. *J. Cell Biol.* 146:493–500. http://dx.doi.org/10.1083/jcb.146.2.493

Schwartz, E.F., C.A. Schwartz, F. Gómez-Lagunas, F.Z. Zamudio, and L.D. Possani. 2006. HgeTx1, the first K^+-channel specific toxin characterized from the venom of the scorpion *Hadrurus gertschi* Soleglad. *Toxicon.* 48:1046–1053. http://dx.doi.org/10.1016/j.toxicon.2006.08.009

Schwartz, E.F., E.M. Capes, E. Diego-García, F.Z. Zamudio, O. Fuentes, L.D. Possani, and H.H. Valdivia. 2009. Characterization of hadrucalcin, a peptide from *Hadrurus gertschi* scorpion venom with pharmacological activity on ryanodine receptors. *Br. J. Pharmacol.* 157:392–403. http://dx.doi.org/10.1111/j.1476-5381.2009.00147.x

Seo, I.R., D.E. Kang, D.W. Song, and D.H. Kim. 2011. Both basic and acidic amino acid residues of $IpTx_a$ are involved in triggering substate of RyR1. *J. Biomed. Biotechnol.* 2011:386384. http://dx.doi.org/10.1155/2011/386384

Shahbazzadeh, D., N. Srairi-Abid, W. Feng, N. Ram, L. Borchani, M. Ronjat, A. Akbari, I.N. Pessah, M. De Waard, and M. El Ayeb. 2007. Hemicalcin, a new toxin from the Iranian scorpion *Hemiscorpius lepturus* which is active on ryanodine-sensitive Ca^{2+} channels. *Biochem. J.* 404:89–96. http://dx.doi.org/10.1042/BJ20061404

Downloaded from http://rupress.org/jgp/article-pdf/147/5/375/1795506/jgp_201511499.pdf by guest on 07 February 2026

Shtifman, A., C.W. Ward, J. Wang, H.H. Valdivia, and M.F. Schneider. 2000. Effects of imperatoxin A on local sarcoplasmic reticulum Ca^{2+} release in frog skeletal muscle. *Biophys. J.* 79:814–827. http://dx.doi.org/10.1016/S0006-3495(00)76338-7

Stern, M.D., and H. Cheng. 2004. Putting out the fire: what terminates calcium-induced calcium release in cardiac muscle? *Cell Calcium.* 35:591–601. http://dx.doi.org/10.1016/j.ceca.2004.01.013

Sutko, J.L., J.A. Airey, W. Welch, and L. Ruest. 1997. The pharmacology of ryanodine and related compounds. *Pharmacol. Rev.* 49:53–98.

Takeshima, H., S. Nishimura, T. Matsumoto, H. Ishida, K. Kangawa, N. Minamino, H. Matsuo, M. Ueda, M. Hanaoka, T. Hirose, et al. 1989. Primary structure and expression from complementary DNA of skeletal muscle ryanodine receptor. *Nature.* 339:439–445. http://dx.doi.org/10.1038/339439a0

Tamura, K., D. Peterson, N. Peterson, G. Stecher, M. Nei, and S. Kumar. 2011. MEGA5: molecular evolutionary genetics analysis using maximum likelihood, evolutionary distance, and maximum parsimony methods. *Mol. Biol. Evol.* 28:2731–2739. http://dx.doi.org/10.1093/molbev/msr121

Tanabe, T., K.G. Beam, J.A. Powell, and S. Numa. 1988. Restoration of excitation-contraction coupling and slow calcium current in dysgenic muscle by dihydropyridine receptor complementary DNA. *Nature.* 336:134–139. http://dx.doi.org/10.1038/336134a0

Tripathy, A., W. Resch, L. Xu, H.H. Valdivia, and G. Meissner. 1998. Imperatoxin A induces subconductance states in Ca^{2+} release channels (ryanodine receptors) of cardiac and skeletal muscle. *J. Gen. Physiol.* 111:679–690. http://dx.doi.org/10.1085/jgp.111.5.679

Valdivia, H.H. 2014. Structural and molecular bases of sarcoplasmic reticulum ion channel function. *In* Cardiac Electrophysiology: From Cell to Bedside. Sixth edition. D.P. Zipes, and J. Jalife, editors. Saunders Elsevier, Philadelphia. 55–69. http://dx.doi.org/10.1016/B978-1-4557-2856-5.00006-6

Valdivia, H.H., M.S. Kirby, W.J. Lederer, and R. Coronado. 1992. Scorpion toxins targeted against the sarcoplasmic reticulum Ca^{2+}-release channel of skeletal and cardiac muscle. *Proc. Natl. Acad. Sci. USA.* 89:12185–12189. http://dx.doi.org/10.1073/pnas.89.24.12185

Wehrens, X.H., S.E. Lehnart, S.R. Reiken, S.X. Deng, J.A. Vest, D. Cervantes, J. Coromilas, D.W. Landry, and A.R. Marks. 2004. Protection from cardiac arrhythmia through ryanodine receptor-stabilizing protein calstabin2. *Science.* 304:292–296. http://dx.doi.org/10.1126/science.1094301

Yan, Z., X.C. Bai, C. Yan, J. Wu, Z. Li, T. Xie, W. Peng, C.C. Yin, X. Li, S.H. Scheres, et al. 2015. Structure of the rabbit ryanodine receptor RyR1 at near-atomic resolution. *Nature.* 517:50–55. http://dx.doi.org/10.1038/nature14063

Yuchi, Z., K. Lau, and F. Van Petegem. 2012. Disease mutations in the ryanodine receptor central region: crystal structures of a phosphorylation hot spot domain. *Structure.* 20:1201–1211. http://dx.doi.org/10.1016/j.str.2012.04.015

Zalk, R., O.B. Clarke, A. des Georges, R.A. Grassucci, S. Reiken, F. Mancia, W.A. Hendrickson, J. Frank, and A.R. Marks. 2015. Structure of a mammalian ryanodine receptor. *Nature.* 517:44–49. http://dx.doi.org/10.1038/nature13950

Zamudio, F.Z., G.B. Gurrola, C. Arévalo, R. Sreekumar, J.W. Walker, H.H. Valdivia, and L.D. Possani. 1997. Primary structure and synthesis of Imperatoxin A ($IpTx_a$), a peptide activator of Ca^{2+} release channels/ryanodine receptors. *FEBS Lett.* 405:385–389. http://dx.doi.org/10.1016/S0014-5793(97)00227-5

Zhou, Q., J. Xiao, D. Jiang, R. Wang, K. Vembaiyan, A. Wang, C.D. Smith, C. Xie, W. Chen, J. Zhang, et al. 2011. Carvedilol and its new analogs suppress arrhythmogenic store overload–induced Ca^{2+} release. *Nat. Med.* 17:1003–1009. http://dx.doi.org/10.1038/nm.2406

Zhu, S., H. Darbon, K. Dyason, F. Verdonck, and J. Tytgat. 2003. Evolutionary origin of inhibitor cystine knot peptides. *FASEB J.* 17:1765–1767.

Downloaded from http://rupress.org/jgp/article-pdf/147/5/375/1795506/jgp_201511499.pdf by guest on 07 February 2026